

# The interplay of phase fluctuations and nodal quasiparticles: ubiquitous Fermi arcs in two-dimensional $d$ -wave superconductors

Xu-Cheng Wang,<sup>1,2</sup> Xiao Yan Xu,<sup>3,4,\*</sup> and Yang Qi<sup>1,2,4,†</sup>

<sup>1</sup>*State Key Laboratory of Surface Physics, Fudan University, Shanghai 200433, China*

<sup>2</sup>*Center for Field Theory and Particle Physics, Department of Physics, Fudan University, Shanghai 200433, China*

<sup>3</sup>*Key Laboratory of Artificial Structures and Quantum Control (Ministry of Education), School of Physics and Astronomy, Shanghai Jiao Tong University, Shanghai 200240, China*

<sup>4</sup>*Hefei National Laboratory, Hefei 230088, China*

(Dated: June 19, 2025)

We propose that the pseudogap and Fermi arcs can universally emerge due to thermal (static) phase fluctuations in the normal state of 2D nodal superconductors. By considering a minimal phenomenological model with spatially fluctuating superconducting pairings, we theoretically investigate the role of superconducting phase fluctuations in generic 2D superconductors with disorder-average technique. It is shown for nodal  $d$ -wave superconductors that phase fluctuations mediate the scattering of  $d$ -wave quasiparticles, smearing out the nodal quasiparticle gap and further leading to pseudogap and Fermi arcs. Moreover, the evolution of Fermi arcs is quantitatively described by two emergent characteristic length scales of the system: one is the finite superconducting correlation length  $\xi(T)$ , and another the nodal BCS coherence length  $\xi_{\text{BCS}}(k)$ . To support our theoretical findings, we numerically report the observation of Fermi arcs in a Hubbard-like model, proposed originally by X. Y. Xu and T. Grover in *Phys. Rev. Lett.* **126**, 217002 (2021), with sign-problem-free determinant quantum Monte Carlo (DQMC) calculations. As far as we noticed, it is the first time in a correlated model that Fermi arcs are identified with unbiased simulations. The numerical results for the scattering rate  $\Gamma_{\text{pf}}$  of Cooper pairs exhibit excellent agreements with our theoretical predictions, where  $\Gamma_{\text{pf}}$  is expected to scale linearly with the inverse superconducting correlation length  $\xi(T)^{-1}$ . This convergence of theory and numerics thereby strongly validates the universal connection between phase fluctuations and Fermi arcs in 2D nodal superconductors.

**Introduction.**— Since its first discovery in underdoped cuprates [1–9] over decades ago, the pseudogap phenomenon has manifested itself in many (quasi) two-dimensional (2D) superconducting materials, including thin-film FeSe [10, 11], layered heavy fermion systems [12–14], and magic angle twisted bilayer graphene [15]. Despite of the varying and intricate material settings, the pseudogap appears to be closely associated with the superconductivity (SC), and seemingly a general phenomenon in 2D superconductors. As a consequence, one prominent explanation to the pseudogap is to treat it as a precursor of superconducting pairing. Recently, a pseudogap originating from strong pairing fluctuations is also confirmed in quantum simulation with ultracold atoms [16], which further extends our understanding of pseudogap to regimes beyond traditional condensed matter system.

In 2D, it is expected that the Berezinskii-Kosterlitz-Thouless (BKT) nature of superconducting transition tends to postpone the complete establishment of phase coherence, thereby suppressing the transition temperature  $T_c$  from a higher mean-field temperature. In this sense, electrons preform pairs above  $T_c$ , leading to a non-zero pairing amplitude, while the phase degrees of Cooper pairs, which are more relevant to the BKT transition, fluctuate strongly, hence contributing to the normal-state physics of 2D superconductors, such as pseudogap. We have previously discussed this general connection between the BKT superconductivity, phase fluctuations,

and pseudogap in our recent work [17].

The Fermi arc [18–21] is another fascinating spectral observation in the pseudogap regime of high- $T_c$  superconductors, e.g. mainly cuprates, where the large Fermi surface breaks into disconnected segments spreading around the nodal points of  $d$ -wave superconductors. The Fermi arc is highly non-trivial in that it clearly violates the Luttinger’s theorem [22], which states that the interacting Fermi surface must be closed and the enclosed volume is directly proportional to the particle density. In a recent numerical study [23], a phenomenological model with pure  $d$ -wave superconducting pairing was investigated, where the authors found solid spectral evidence for the existence of pseudogap and Fermi arcs caused by superconducting fluctuations. An important implication of their results is that the pseudogap and accompanying Fermi arcs require neither the strong correlation nor the presence of competing order, which again stressed the close connection of Fermi arcs and the superconductivity itself. Other relevant works along this stream include Refs. [24–26], where the role of phase fluctuations was investigated specifically for underdoped cuprates. Based on these early studies on specific materials, it is thereby plausible to argue that the Fermi arcs shall naturally emerge in the normal state of SC, and appear to be ubiquitous in 2D nodal superconductors due to the universal interplay of phase fluctuations and nodal quasiparticles.

In this article, we manage to first theoretically establish this connection between thermal (static) phase fluc-

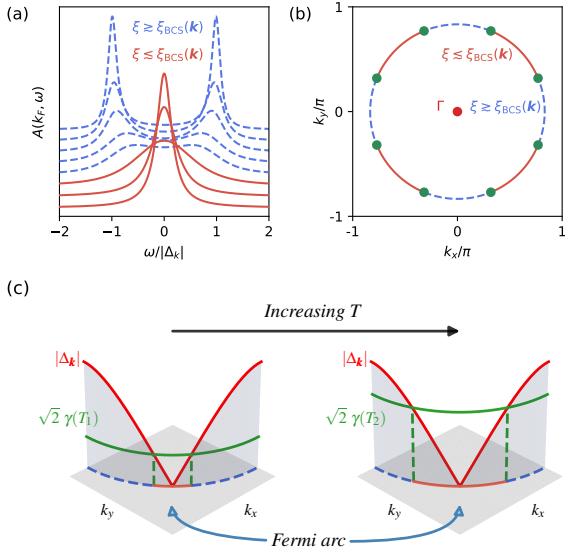


FIG. 1. (a) Evolution of single-particle spectral weights  $A(k_F, \omega) = -2\text{Im}[G(k_F, \omega)]$  as a competition of BKT correlation length  $\xi$  and nodal BCS coherence length  $\xi_{\text{BCS}}(k)$ . (b) Schematic plot of the Fermi arcs formation. A circular Fermi surface has been adopted for simplicity. The Fermi surface survives for momenta satisfying  $\xi \lesssim \xi_{\text{BCS}}(k)$ , while for momenta with  $\xi \gtrsim \xi_{\text{BCS}}(k)$  the spectra are pseudogapped, leading to the emergence of Fermi arcs. (c) Evolution of Fermi arcs with increasing temperature  $T$ . The arcs involve those momenta satisfying  $\gamma(T)/|\Delta_k| \gtrsim \frac{1}{\sqrt{2}}$  up to the leading order of perturbation theory. It is assumed that the pair-scattering rate  $\gamma$  is uniform on the circular Fermi surface.

tuations and Fermi arcs in 2D nodal superconductors. The effects of phase fluctuations on electrons are taken into account by expanding the correlation functions perturbatively over SC pairing amplitude and analytically averaging over spatially fluctuating pairings. Our calculations reveal that, due to the scattering events mediated by the fluctuating phase degrees of SC, the BCS quasiparticles acquire a finite life-time proportional to  $\gamma(T)^{-1} \sim \xi(T)$  in the SC normal state. Here,  $\gamma(T)$  denotes the pair-scattering rate and  $\xi(T)$  the BKT superconducting correlation length. It is further shown that, the competition between  $\gamma(T)$  and the  $d$ -wave pairing gap  $\Delta_k$ , or equivalently the correlation length  $\xi(T)$  and the nodal BCS coherence length  $\xi_{\text{BCS}}(k) = \frac{v_F}{\pi|\Delta_k|}$ , gives rise to the emergence of pseudogap and Fermi arcs in a unified picture. The pseudogap generally manifests when  $\xi(T) \gtrsim \xi_{\text{BCS}}(k)$ , and the anisotropy of nodal  $\Delta_k$  and  $\xi_{\text{BCS}}(k)$  guarantees the presence of Fermi arcs, as shown in Fig. 1.

Furthermore, in order to support our theory numerically, we report direct observations of Fermi arcs in a Hubbard-like model with sign-problem-free determinant Quantum Monte Carlo (DQMC) simulations. Both  $\gamma(T)$  and  $\xi(T)$  are independently determined for the inter-

acting model, thereby providing solid evidence on the phase-fluctuation-driven Fermi arcs. Our findings also imply the possibility of numerically observing Fermi arcs in many other 2D models with nodal superconductivity, and provide theoretical supports for detecting Fermi arcs empirically with spectroscopic measurements in (quasi) 2D nodal superconducting materials, in addition to the cuprate family which have been extensively studied.

*Phase fluctuations and Fermi arcs.*— Our theoretical examinations of phase fluctuations start from a phenomenological Hamiltonian with a generic form of superconducting pairing as below,

$$H = \sum_{\sigma} \int d^2\mathbf{r} \psi_{\sigma}^{\dagger}(\mathbf{r}) \left( -\frac{\nabla^2}{2m} - \mu \right) \psi_{\sigma}(\mathbf{r}) + \int d^2\mathbf{r} d^2\mathbf{s} \Delta(\mathbf{r}, \mathbf{s}) \psi_{\uparrow}^{\dagger}(\mathbf{r} + \mathbf{s}/2) \psi_{\downarrow}^{\dagger}(\mathbf{r} - \mathbf{s}/2) + \text{h.c.} \quad (1)$$

The superconducting order parameters  $\Delta(\mathbf{r}, \mathbf{s})$  are allowed to exhibit a general dependence on the intrinsic momentum,  $\int d^2\mathbf{s} e^{-i\mathbf{ps}} \Delta(\mathbf{r}, \mathbf{s}) = \Delta(\mathbf{r}) \varphi(\mathbf{p})$ , where  $\varphi(\mathbf{p})$  denotes the form factor of pairing, e.g.  $\varphi_d(\mathbf{p}) = (p_x^2 - p_y^2)/p^2$  for the  $d_{x^2-y^2}$  pairing. Throughout this work, we assume that: (1) Due to the BKT nature of 2D superconducting transition, the phase fluctuations of  $\Delta(\mathbf{r}, \mathbf{s})$  dominate the low-energy physics above  $T_c$ , while its amplitude  $|\Delta(\mathbf{r}, \mathbf{s})|$  maintains the mean-field value  $\Delta_0$ . This is partially supported by the anomalously small superfluid density  $\rho_s$  observed in 2D superconductors [27–29], e.g. cuprates. The small value of  $\rho_s$  implies that the temperature  $T_\theta \approx \rho_s/m^*$  associated with phase fluctuations is of the same order as the superconducting temperature  $T_c$ , which suggests that the phase fluctuations play a crucial role in the thermodynamics near  $T_c$ . (2) The superconducting fluctuations in the temporal direction are neglectable compared with the spatial ones. Namely, we consider here only the static fluctuations. This can be argued from the fact that as the BKT transition point of SC is approached from higher temperatures, the spatial correlation length  $\xi$  formally diverges while the correlation in the imaginary-time direction is bounded by a finite inverse temperature  $\beta = (k_B T)^{-1} \ll \xi/v_F$ . Hence for the low-energy theory with a cutoff length scale  $a$  satisfying  $v_F\beta < a < \xi$ , all temporal fluctuations of  $\Delta(\mathbf{r}, \mathbf{s})$  are effectively integrated out.

Under these assumptions, the Hamiltonian in Eq. (1) can be regarded as a low-energy effective model where free electrons experience a spatially disordered pairing potential. With certain fixed configurations of  $\Delta(\mathbf{r}, \mathbf{s})$ , one can thus unambiguously solve the correlation functions of electrons by adopting perturbative expansions over  $\Delta_0$  (we assume  $\Delta_0$  is real-valued and sufficiently small as compared to the Fermi energy such that  $\Delta_0/E_F \ll 1$ ). The effects of phase fluctuations are then taken into account through averaging over the fluctuat-

ing configurations of  $\{\Delta(\mathbf{r}, \mathbf{s})\}$  according to the following conditions of disorder average,

$$\overline{\Delta(\mathbf{r})} = \overline{\Delta^*(\mathbf{r})} = 0, \quad (2a)$$

$$\overline{\Delta(\mathbf{r})\Delta^*(\mathbf{r}')} = \Delta_0^2 g(|\mathbf{r} - \mathbf{r}'|/\xi), \quad (2b)$$

where the overline represents the average over fluctuating pairing configurations.  $g(x)$  is a general scaleless function that exponentially decays from  $g(0) = 1$  to 0 as  $x \gg 1$ . Eq. (2a) indicates that the superconducting order is not permitted to develop locally in the normal state as expected, while the two-point correlation in Eq. (2b) survives and decays with the distance, characterized by the superconducting correlation length  $\xi$ . For 2D superconductors, the superconducting transition generally falls into the BKT universality class, and therefore  $\xi$  follows a BKT scaling form as  $\xi(T) \sim \exp(bt_r^{-1/2})$  [30, 31], where  $b$  is a non-universal constant and  $t_r = (T - T_c)/T_c$  denotes the reduced temperature.

Following the scheme outlined above, we can evaluate correlations of any order in principle within the perturbation theory. In this work, we mainly focus on the single-particle properties, e.g. the electronic self-energy and spectrum, of  $d$ -wave SC. For details of the theoretical calculations, readers may refer to Refs. [17, 32]. It turns out that in the vicinity of superconducting transition  $T \gtrsim T_c$  with  $k_F \xi \gg 1$ , the electronic self-energy acquires an intuitive form to the leading order as,

$$\Sigma(\mathbf{k}, \omega) = \frac{|\Delta_{\mathbf{k}}|^2}{\omega + \xi_{\mathbf{k}} + 2i\gamma_{\mathbf{k}}}. \quad (3)$$

We have defined the  $d$ -wave gap function  $\Delta_{\mathbf{k}} = \Delta_0 \varphi_d(\mathbf{k})$  and the phase-fluctuation-driven scattering rate  $\gamma_{\mathbf{k}} = v_{\mathbf{k}}/2\xi$  with  $v_{\mathbf{k}}$  the electronic velocity. Eq. (3) then describes a standard BCS-like self-energy corrected by the finite life-time of Cooper pairs, which contributes as a well-defined imaginary part of the self-energy. Moreover, the retarded Green's function follows from the self-energy through the Dyson series  $G(\mathbf{k}, \omega) = [\omega - \xi_{\mathbf{k}} - \Sigma(\mathbf{k}, \omega)]^{-1}$ , which exhibits complex poles [32] at

$$E_{\pm}(\mathbf{k}) = -i\gamma_{\mathbf{k}} \pm \sqrt{(\xi_{\mathbf{k}} + i\gamma_{\mathbf{k}})^2 + |\Delta_{\mathbf{k}}|^2}. \quad (4)$$

Consequently, Eq. (4) serves as a conceivable extension to the dispersion of BCS quasiparticle in the presence of phase fluctuations. Specially, if we consider electrons at the Fermi surface, Eq. (4) becomes

$$E_{\pm} = -i\gamma \pm \sqrt{|\Delta_{\mathbf{k}}|^2 - \gamma^2}, \quad (5)$$

with the associated pair-scattering rate  $\gamma = v_F/2\xi$ . It is insightful to note that this square-root feature of dispersion reminds us of the order-2 exceptional points (EPs) observed in Dirac semimetals [33] and Kondo lattice systems [34], where bulk Fermi arcs are generally predicted

due to the presence of such topological EPs according to the topological band theory [33, 35–37]. Broadly speaking, although in our case the microscopic Hamiltonian Eq. (1) is Hermitian, averaging it over fluctuating pairing potentials results in an effective non-hermitian description to the problem at the single-particle level, which hosts EPs:  $\{\mathbf{k} \in \text{BZ} \mid \xi_{\mathbf{k}} = 0, |\Delta_{\mathbf{k}}| = \gamma\}$ . Therefore, the Fermi arcs, which are protected by the topological EPs, are expected to naturally emerge in phase-disordered superconductors, spreading around the superconducting nodes and terminating at these EPs.

To make this argument more explicit, we explore the implications of self-energy Eq. (3) in more detail. It is found that Eq. (3) and Eq. (5) provide a unified description of the crossover from BCS-like physics to high-temperature Fermi liquid behavior. Recall that the real components of the Green's function poles in Eq. (5) denote the quasiparticle energy, while the imaginary parts characterize the inverse life-time of quasiparticle. For temperatures  $T$  above and close to  $T_c$ , the BKT correlation length  $\xi(T)$  is finite but still remains long-ranged such that  $\gamma(T) \lesssim |\Delta_{\mathbf{k}}|$ . It is thus insufficient for the phase fluctuations to fully suppress the coherent pairing of electrons, and hence the Cooper pairs still survive up to a finite life-time  $\gamma^{-1}(T) \sim \xi(T)$ . In this case, the two Green's function poles manifest at opposite frequencies, i.e.  $\text{Re}[E_+] = -\text{Re}[E_-] \neq 0$  as a reminiscence of coherent peaks. At higher temperatures where the phase fluctuations prevail with short-ranged  $\xi(T)$  and  $\gamma(T) \gtrsim |\Delta_{\mathbf{k}}|$ , both of these two quasiparticle modes settle at the Fermi energy  $\omega = 0$ , i.e.  $\text{Re}[E_{\pm}] = 0$  which corresponds to a Fermi liquid. Finally at sufficiently high temperatures, the ideal dispersion of free electron is recovered. In conclusion, the phase fluctuations proliferate as the temperature increases from  $T_c$ , and accordingly the system undergoes a smooth crossover from the BCS physics to a Fermi liquid. This crossover, illustrated in Fig. 1(a), can be tracked by the comparison of  $\gamma(T)$  and  $|\Delta_{\mathbf{k}}|$ , or equivalently the competition of BKT correlation length  $\xi(T)$  and the BCS coherence length of nodal SC,

$$\xi_{\text{BCS}}(\mathbf{k}) = \frac{v_F}{\pi|\Delta_{\mathbf{k}}|}, \quad (6)$$

which characterizes the spatial size of Cooper pair in the weak-coupling BCS theory [38].

Moreover, it is realized that these characteristic length scales  $\xi(T)$  and  $\xi_{\text{BCS}}(\mathbf{k})$  further account for the evolution of pseudogap and Fermi arcs in the intermediate regime of the crossover. A straightforward leading-order calculation [32] reveals that for  $\gamma(T)/|\Delta_{\mathbf{k}}| < \frac{1}{\sqrt{2}}$ , the pseudogap emerges in the electronic single-particle spectrum, and is not completely closed until

$$\frac{\gamma(T)}{|\Delta_{\mathbf{k}}|} = \frac{1}{\sqrt{2}}, \quad \text{i.e.} \quad \frac{\xi_{\text{BCS}}(\mathbf{k})}{\xi(T)} = \frac{\sqrt{2}}{\pi}. \quad (7)$$

Taking into account the anisotropy of the pairing gap

$|\Delta_{\mathbf{k}}|$ , this analysis intuitively explains the presence of Fermi arcs as shown in Fig. 1(b)(c). We again consider the electrons with Fermi momentum, and adopt a circular Fermi surface for convenience. At certain temperature  $T$ , the correlation length  $\xi$  and pair-scattering rate  $\gamma$  are uniform on the Fermi surface, while the pairing gap  $\Delta_{\mathbf{k}}$  and hence the BCS coherence length  $\xi_{\text{BCS}}(\mathbf{k})$  are highly anisotropic. For those momenta near anti-nodes which experience large  $|\Delta_{\mathbf{k}}|$ , the spectrum is pseudogapped. Otherwise for momenta near the nodes, the spectrum remains metallic, and a Fermi surface partially survives at these momenta. As the temperature increases, the strong phase fluctuations lead to a rapid decrease in  $\xi(T)$  and thus a significant increase in  $\gamma(T)$ , causing the arcs to grow. Eventually at sufficiently high temperatures, the large Fermi surface is recovered, and this evolution is also demonstrated in Fig. 1(c). The discussion above hence establishes a universal connection between the phase fluctuations, pseudogap, and Fermi arcs in 2D nodal superconductors.

It is worth noting that the analyses above are based on the perturbative expansion over the pairing amplitude  $\Delta_0$  and the assumption of large correlation length  $k_F \xi \gg 1$ . As inferred from Eq. (7), ensuring the validness of our theory in the pseudogap regime further requires that  $\xi \sim \xi_{\text{BCS}} \gg k_F^{-1}$ , which also implies a small  $\Delta_0$ . Consequently, it is reasonable to apply our theory to weak-coupling 2D superconducting systems with weak phase fluctuations. Moreover, the argument for the Fermi arcs is in principle universally applicable to 2D superconductors with generic pairing symmetries, although we have mostly emphasized on the case of  $d$ -wave SC. Therefore, the Fermi arcs are expected to be generally present for 2D superconductors with nodes.

*Numerical studies.*— To support our theoretical findings on the phase-fluctuation-driven Fermi arcs, we investigate a Hubbard-like model on square lattice with determinant Quantum Monte Carlo (DQMC) simulation. The model we studied here was proposed by Xu and Grover in Ref. [39], the ground state of which has been proved to exhibit a competition between nodal  $d$ -wave superconductivity (dSC) and antiferromagnetism (AFM). This model explicitly involves band electrons  $c_{i,\sigma}(c_{i,\sigma}^\dagger)$ , which live on the vertices  $\{i\}$  of the square lattice, and the fluctuating  $\mathbb{U}(1)$  rotors  $e^{i\theta_{ij}}$  living on the nearest-neighbor bonds  $\{ij\}$ . The Hamiltonian is given by  $H = H_t + H_U + H_V + H_{XY}$ , where  $H_t + H_U = -t \sum_{\langle ij \rangle, \sigma} (c_{i\sigma}^\dagger c_{j\sigma} + \text{h.c.}) + \frac{1}{2} U \sum_i (\rho_{i\uparrow} + \rho_{i\downarrow} - 1)^2$  denotes the standard Hubbard model at half-filling with nearest-neighbor hoppings, and  $\rho_{i\sigma} = c_{i\sigma}^\dagger c_{i\sigma}$ .  $H_V = V \sum_{\langle ij \rangle} [\tau_{ij} e^{i\theta_{ij}} (c_{i\uparrow}^\dagger c_{j\downarrow}^\dagger - c_{i\downarrow}^\dagger c_{j\uparrow}^\dagger) + \text{h.c.}]$  is the coupling between electrons and rotors in the  $d$ -wave pairing channel, where  $\tau_{ij} = 1$  for bonds  $\langle ij \rangle$  along the  $x$ -axis and  $-1$  for bonds along the  $y$ -axis.  $H_{XY} = K \sum_{\langle ij \rangle} \hat{L}_{ij}^2 - J \sum_{\langle ijk \rangle} \cos(\theta_{ij} - \theta_{jk})$  governs the dynamics of rotors and a self-interaction term is included

resembling the one in the quantum rotor model [40].  $\hat{L}_{ij}$  denotes the canonical momentum of rotor, and  $\sum_{\langle ijk \rangle}$  sums over pairs of rotors which share the same lattice site  $j$ . Note that this model preserves all the symmetries present in the half-filled Hubbard model, including the spin-rotation  $\mathbb{SU}(2)$ , particle-hole and, especially, the  $\mathbb{U}(1)$  charge symmetry, which leaves it possible for us to investigate the BKT superconducting transition at finite temperatures. Furthermore, what is technically important is that the model is free of the infamous sign problem due to the presence of an anti-unitary symmetry [41]  $\mathcal{U}$ :  $c_{i,\sigma} \rightarrow \sigma (-)^i c_{i,-\sigma}^\dagger$ ,  $\sqrt{-1} \rightarrow -\sqrt{-1}$  and  $\mathcal{U}^2 = -1$ . A complete ground-state phase diagram has been established in Ref. [39]: it hosts three distinct phases, including a nodal  $d$ -wave phase, which is the focus of our interest here, an antiferromagnet, and an intervening phase where AFM and nodeless dSC coexist.

In order to detect the Fermi arcs and examine the role of phase fluctuations, we simulate the model at finite temperatures using DQMC. Details about the DQMC algorithm and its implementation to the present model can be found in [32, 42]. Unless otherwise specified, we set the imaginary-time spacing  $\Delta\tau$  equal to  $0.025/t$  for maintaining a controllable systematic error, and work with the lattice size  $L$  ranging from 12 to 20. For all our presented results, we have set  $t = 1$ ,  $U/t = 4$ ,  $V/t = 1$ , and  $K/t = J/t = 1/2$ . This set of parameters realizes a nodal  $d$ -wave superconductor, and importantly, there is no presence of long-range AFM order within the temperature range that we considered [32].

In Fig. 2, we show the observation of Fermi arcs in the electronic single-particle spectrum of the interacting model. The single-particle spectra are extracted through the stochastic analytic continuation (SAC) [32, 43, 44] calculations from the imaginary-time Green's functions obtained by standard Monte Carlo samplings. As shown in Fig. 2(b), in the dSC phase, a nodal superconducting gap clearly manifests in the single-particle spectrum, and the extraction of gap function in Fig. 2(d) warrants the  $d_{x^2-y^2}$  symmetry of the gap. As the system enters into the normal state with increased temperature, the Fermi arcs gradually spread to the antinodal regions, illustrated as red curves in Fig. 2(b). This evolution of pseudogap and Fermi arcs shall be well attributed to the enhanced phase fluctuations, which will be verified in the following content.

First of all, the SC transition temperature  $T_c$  is determined as follows. We define the  $d$ -wave pairing order parameter in terms of both fermionic,  $\Delta_d = \frac{1}{2L^2} \sum_{\langle ij \rangle} \tau_{ij} (c_{j\downarrow} c_{i\uparrow} - c_{j\uparrow} c_{i\downarrow})$ , and bosonic,  $\alpha = \frac{1}{2L^2} \sum_{\langle ij \rangle} e^{i\theta_{ij}}$ , degrees of freedom. The associated static pairing correlation  $P_d = \langle \Delta_d \Delta_d^\dagger + \Delta_d^\dagger \Delta_d \rangle$  and  $\alpha^2 = \frac{1}{4L^4} \sum_{\langle ij \rangle, \langle kl \rangle} \langle e^{i\theta_{ij}} e^{-i\theta_{kl}} \rangle$  are then measured and displayed in Fig. 3(a)(c). Following the standard procedure of data collapse [32], we determine in Fig. 3(b)(d) the

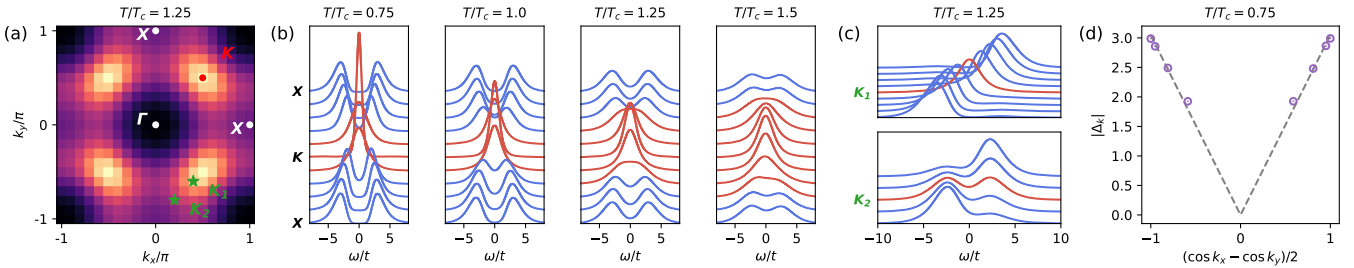


FIG. 2. Observation of Fermi arcs in the Hubbard-like model using DQMC. (a) Green's function  $\beta G(\mathbf{k}, \beta/2)$  as an estimation of the single-particle spectral function  $A(\mathbf{k}, \omega = 0)$  in the normal state  $T/T_c = 1.25$  with lattice size  $L = 20$ . The nodal point is labeled as  $K$ , and the anti-nodal point as  $X$ . (b) Single-particle spectral function  $A(\mathbf{k}, \omega)$  along the node-antinode line  $X-K-X$  for varying  $T$ . The red curves outline the shape of Fermi arcs, and the length of Fermi arcs grows with increasing temperature. (c) Single-particle spectral function  $A(\mathbf{k}, \omega)$  along the momentum path perpendicular to the Fermi surface in the normal state  $T/T_c = 1.25$ . The momentum paths intersect with the Fermi surface at  $K_1$  and  $K_2$  respectively, marked out as green stars in Fig. 2(a). At this temperature,  $K_1$  belongs to the Fermi arc while  $K_2$  is not. (d)  $d$ -wave gap function  $|\Delta_{\mathbf{k}}|$  extracted directly from the electronic single-particle spectrum in the dSC phase.

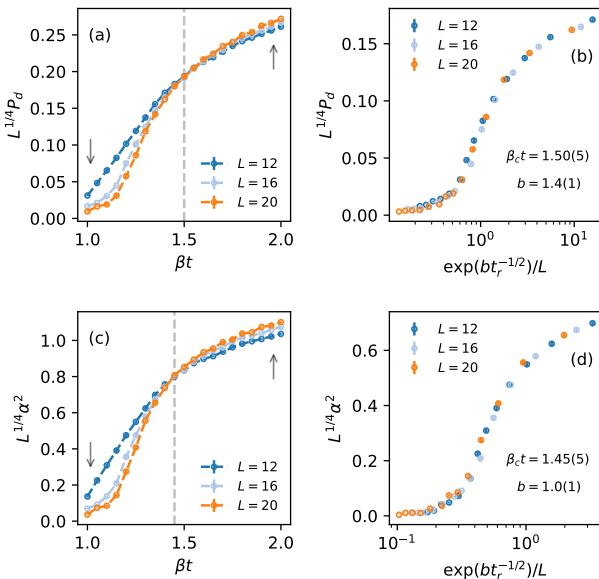


FIG. 3. Data collapse to determine the BKT transition temperature  $T_c$  and the superconducting correlation length  $\xi(T)$ . (a)(c) Static  $d$ -wave pairing correlation  $P_d$  and  $\alpha^2$  for varying inverse temperature  $\beta$  and system size  $L$ . According to the finite-size-scaling theory, the transition temperature  $\beta_c$  is marked as the temperature where  $L^n P_d(L, \beta)$ , or  $L^n \alpha^2(L, \beta)$ , for all  $L$  converge, which is noted as grey dashed line in (a)(c). We have fixed the critical exponent  $\eta(T_c) = 1/4$  for the BKT transition [30, 31]. (b)(d) Data collapse of  $P_d$  and  $\alpha^2$ . It is obtained that  $\beta_{ct} = 1.50(5)$ ,  $b = 1.4(1)$  for  $P_d$ , and  $\beta_{ct} = 1.45(5)$ ,  $b = 1.0(1)$  for  $\alpha^2$ . The superconducting correlation length is then determined through  $\xi(T) \sim \exp(bt_r^{-1/2})$  with  $t_r = T/T_c - 1$ , up to a non-universal prefactor.

inverse critical temperature  $\beta_c$  and meanwhile the BKT correlation length  $\xi(T) \sim \exp(bt_r^{-1/2})$ . For  $P_d$ , the data collapse yields  $\beta_{ct} = 1.50(5)$ ,  $b = 1.4(1)$ , and for  $\alpha^2$ ,  $\beta_{ct} = 1.45(5)$ ,  $b = 1.0(1)$ . It turns out that the SC tran-

sition temperature  $T_c = 1/\beta_c$  obtained from  $P_d$  is consistent with that from  $\alpha^2$  within the estimated errorbar. In contrast, the non-universal factor  $b$  varies for  $P_d$  and  $\alpha^2$ . This discrepancy arises from the fact that the dSC order detected in the electronic system is actually induced by the symmetry breaking of bosonic rotors. Therefore, focusing on the electronic side of the model, we adopt the transition temperature  $\beta_c = 1.50(5)$  and  $b = 1.4(1)$  according to the data collapse of  $P_d$ . The temperature-dependent BKT correlation length is then determined via  $\xi(T) \sim \exp(bt_r^{-1/2})$  up to a prefactor.  $\xi(T)$  is crucial in quantifying superconducting fluctuations and serves as the prior input of our theory.

Recall that in the preceding section, we have shown that the self-energy Eq. (3) takes into account the normal-state phase fluctuations, which account for the evolution of pseudogap and Fermi arcs. To directly validate Eq. (3) for the interacting model, we managed to explicitly extract the electronic self-energy  $\Sigma(\omega)$  from the single-particle spectrum  $A(\omega)$  obtained by SAC. This is realized by noting that  $A(\omega) = -2\text{Im}[G(\omega)]$  and  $\text{Re}[G(\omega)]$  can be computed from  $A(\omega)$  based on the Kramers-Kronig relation [45]. Then the desired self-energy is related to the complex Green's function through  $\Sigma(\omega) = [G^{(0)}]^{-1} - G^{-1}$ , where  $G^{(0)} = 1/(\omega - \xi_k + i0^+)$  denotes the Green's function of free band electron.

In Fig. 4, we show the electronic single-particle spectrum at the antinode obtained from SAC, and the corresponding self-energy evaluated. The evolution of pseudogap with respect to temperature is clearly illustrated in Fig. 4(a), and it is inspiring that the imaginary part of the self-energy in Fig. 4(b) indeed behaves as what we expected theoretically in Eq. (3). For the antinodal electron with temperature  $T$  near  $T_c$  in the normal state,  $\text{Im}[\Sigma(\omega)]$  exhibits a pronounced peak at the Fermi energy  $\omega = 0$ , subject to a finite broadening caused by the scatterings of Cooper pairs. As  $T$  increases, the self-

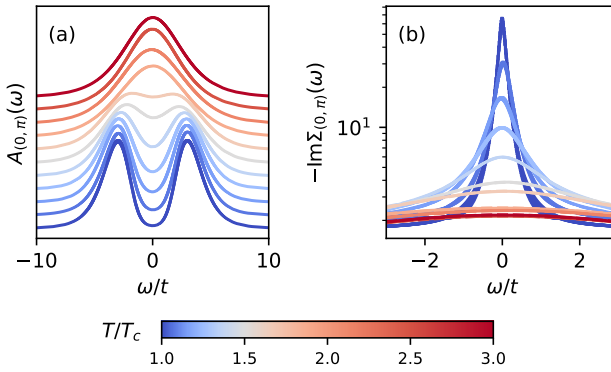


FIG. 4. (a) Antinodal pseudogap in the normal state, extracted by combining DQMC and SAC on a  $L = 20$  lattice. (b) Electronic self-energy evaluated from the single-particle spectrum in Fig. 4(a). The y-axis is log-scaled for better visualization. As predicted in Eq. (3), the imaginary part of self-energy exhibits a pronounced peak at the Fermi energy  $\omega = 0$  for antinodes near  $T_c$ , whose broadening shall be given by  $\gamma_k(T)$  ideally.

energy peak gets damped until completely destroyed by phase fluctuations, and meanwhile the pseudogap closes at  $T/T_c \sim 2$  eventually.

To proceed, we fit the self-energies  $\Sigma(\omega)$  in Fig. 4(b) according to

$$\Sigma(\omega) = \frac{\tilde{\Delta}^2}{\omega + 2i\Gamma_{\text{pf}}} - i\Gamma_0, \quad (8)$$

which almost resembles the self-energy in Eq. (3) with  $\xi_k = 0$  for electrons at the Fermi energy.  $\Gamma_{\text{pf}}$  is interpreted as the pair-scattering rate due to phase fluctuations, i.e.  $\Gamma_{\text{pf}}(T) \sim v_F \xi^{-1}$ , and  $\Gamma_0$  can be regarded as a Fermi-liquid-like renormalization.  $\tilde{\Delta}$  denotes the renormalized superconducting gap for certain momentum on the Fermi surface. It turns out that this form of self-energy is also widely accepted as a working-assumption in dealing with angle-resolved photoemission data of realistic high- $T_c$  materials [46, 47]. In practice, we fit the imaginary-part of self-energies for frequencies below the dSC gap  $\Sigma(|\omega| \lesssim |\Delta_k|)$ , as this region dominates the low-energy evolution of the pseudogap. The fittings are excellent that the fitted curves coincide with the self-energies within errorbars for a broad range of temperatures.

In Fig. 5(a), we plot the pair-scattering rate  $\Gamma_{\text{pf},\Sigma}$ , fitted from the self-energies, with respect to the BKT correlation length  $\xi(T)$  previously obtained through data collapse. Electrons at the Fermi energy but with varying momenta near the antinode are considered. Ideally it is expected that  $\Gamma_{\text{pf},\Sigma} \sim \xi^{-1}$  validating the prediction of our theory. As indicated by the dashed lines in Fig. 5(a), this linear relation between  $\Gamma_{\text{pf}}$  and  $\xi^{-1}$  is well established over a broad range of temperatures  $1 < T/T_c < 1.5$ , with the exception of a finite residual

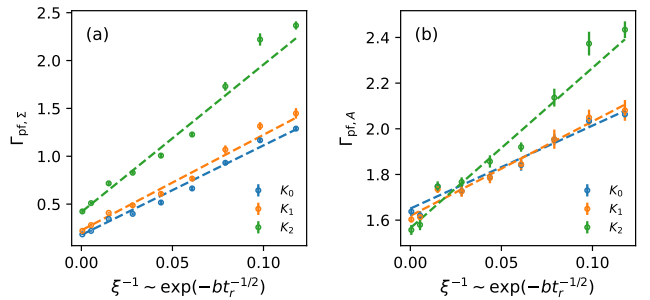


FIG. 5. Pair-scattering rate  $\Gamma_{\text{pf}}$  extracted by (a) fitting the electronic self-energy  $\Sigma(\omega)$  to obtain  $\Gamma_{\text{pf},\Sigma}$ , and (b) identifying the half-width of BCS quasiparticle peaks  $A(|\omega| \sim |\Delta_k|)$  as  $\Gamma_{\text{pf},A}$ . The dashed lines are linear fittings of  $\Gamma_{\text{pf}}$  with respect to  $\xi^{-1}$ . The DQMC data contributing to the evaluations of electronic spectra and self-energies are obtained on a  $L = 20$  lattice with  $1 < T/T_c < 1.5$ . The temperature-dependent correlation length  $\xi(T)$  was previously determined in Fig. 3 through data collapse with  $\beta_c = 1.50(5)$  and  $b = 1.4(1)$ . We have focused on the electronic momenta satisfying  $\xi_k = 0$  and in the neighborhood of antinodes. Specifically, the momenta are chosen as  $K_n = K_0 + n\Delta k$  with  $K_0 = (0, \pi)$  and the momentum shift  $\Delta k = (2\pi/L, -2\pi/L)$ .

observed at  $T_c$  with vanishing  $\xi^{-1}$ . Such residual of pair-scattering rate, denoted as  $\Gamma_{\text{res}}$ , is a direct consequence of the finite half-width of  $A(|\omega| \sim |\Delta_k|)$  at  $T_c$  in Fig. 4(a) and the finite broadening of self-energy at  $T_c$  in Fig. 4(b). The origin of  $\Gamma_{\text{res}}$  shall be attributed to multiple factors. First of all, for a finite-size system, the correlation length is naturally bounded by the system size  $L$ , resulting in a possible finite  $\xi$  at  $T_c$  and hence finite  $\Gamma_{\text{res}}$ . Furthermore, the repulsion among electrons gives rise to additional scatterings of them, and may renormalize the BCS quasiparticle with additional broadening at  $T_c$ . It is also inspired by the studies on short-ranged charge [48, 49] and spin [50–52] correlations that phase fluctuations beyond the leading order of perturbation theory may also contribute to the finite  $\Gamma_{\text{res}}$  even at  $T_c$ .

Regardless of the various reasons contributing to the residual broadening at  $T_c$ , the evolution of  $\Gamma_{\text{pf},\Sigma}(T)$  in the normal state matches the theoretical prediction well, exhibiting a linear dependence on  $\xi(T)^{-1}$ . As a supplementary confirmation, we note that in the weakly fluctuating regime  $\gamma/|\Delta_k| \ll 1$ , the half-width of BCS quasiparticle weight  $A(|\omega| \sim |\Delta_k|)$  in the normal state, Fig. 4(a), is approximately given by the pair-scattering rate  $\gamma$  [32]. It is thus plausible to approximate the pair-scattering rate, which we denote as  $\Gamma_{\text{pf},A}$  in this case, as the half-width of BCS quasiparticle weights near  $|\omega| \sim |\Delta_k|$ . Following the similar procedure as for  $\Gamma_{\text{pf},\Sigma}$ , we fit the half-width of spectral weights and again observe in Fig. 5(b) the linear relationship between  $\Gamma_{\text{pf},A}$  and  $\xi^{-1}$ .

Combining all these facts, we finally conclude that the presence of normal-state phase fluctuations in 2D generally introduce scatterings to the BCS quasiparti-

cle. The associated BKT correlation length  $\xi(T)$  gives rise to the broadening of self-energies  $\gamma \sim \xi^{-1}$ , and its competition with the BCS coherence length  $\xi_{\text{BCS}}$  further dominates the evolution of pseudogap and Fermi arcs in 2D superconductors. This outlined mechanism is robust against moderate electron rupulsion as verified in our Hubbard-like model by DQMC, and therefore the phase-fluctuation-driven Fermi arcs shall be considered general for 2D nodal superconductors.

*Conclusion and discussions.*— In summary, we have shown that the normal-state phase fluctuations are essential in understanding the formation of pseudogap in 2D superconductors. Furthermore, for nodal systems, the interplay of phase fluctuations and nodal quasiparticles gives birth to Fermi arcs in a quite general manner. We quantitatively confirm our theoretical predictions by conducting a sign-problem-free DQMC study on a Hubbard-like model with dSC ground state. The evolution of Fermi arcs is evidently observed in the normal state of the model, and the extracted pair-scattering rates align precisely with our theory, scaling linearly with respect to the inverse BKT correlation length  $\xi(T)^{-1}$ .

The methodology we followed here implies a reliable approach to analyzing phase fluctuations with generic superconducting pairing symmetries, and can be also readily extended to address problems concerning static disorders and other fluctuating orders at finite temperatures. Given the plausible role of spin fluctuations in inducing the unconventional pairing in high- $T_c$  SC [53, 54], it is both intriguing and feasible to consider the coexistence of short-ranged AFM and SC order on the same footing within our theoretical framework. Moreover, beyond the single-particle property explored primarily in this study, it is equally compelling to examine the two-particle properties of such phase-disordered superconductor, such as its response to external magnetic probes. All these directions will guide our future works.

*Acknowledgements.*— Y.Q. is supported by National Natural Science Foundation of China (NSFC) through Grant Nos. 11874115 and 12174068. X.Y.X. acknowledges the support of the National Key R&D Program of China (Grant No. 2022YFA1402702, No. 2021YFA1401400), the National Natural Science Foundation of China (Grants No. 12447103, No. 12274289), the Innovation Program for Quantum Science and Technology (under Grant No. 2021ZD0301902), Yangyang Development Fund, and startup funds from SJTU. The authors also appreciate Beijing PARATERA Tech CO., Ltd. for providing the HPC resources which have contributed to the computational results presented in this work.

<sup>†</sup> qiyang@fudan.edu.cn

- [1] H. Alloul, T. Ohno, and P. Mendels, *Phys. Rev. Lett.* **63**, 1700 (1989).
- [2] D. S. Marshall, D. S. Dessau, A. G. Loeser, C.-H. Park, A. Y. Matsuura, J. N. Eckstein, I. Bozovic, P. Fournier, A. Kapitulnik, W. E. Spicer, and Z.-X. Shen, *Phys. Rev. Lett.* **76**, 4841 (1996).
- [3] C. Renner, B. Revaz, J.-Y. Genoud, K. Kadowaki, and O. Fischer, *Phys. Rev. Lett.* **80**, 149 (1998).
- [4] T. Timusk and B. Statt, *Rep. Prog. Phys.* **62**, 61 (1999).
- [5] P. A. Lee, N. Nagaosa, and X.-G. Wen, *Rev. Mod. Phys.* **78**, 17 (2006).
- [6] M. R. Norman, *Science* **332**, 196 (2011).
- [7] M. Hashimoto, I. M. Vishik, R.-H. He, T. P. Devereaux, and Z.-X. Shen, *Nat. Phys.* **10**, 483 (2014).
- [8] N. J. Robinson, P. D. Johnson, T. M. Rice, and A. M. Tsvelik, *Rep. Prog. Phys.* **82**, 126501 (2019).
- [9] J. A. Sobota, Y. He, and Z.-X. Shen, *Rev. Mod. Phys.* **93**, 025006 (2021).
- [10] B. L. Kang, M. Z. Shi, S. J. Li, H. H. Wang, Q. Zhang, D. Zhao, J. Li, D. W. Song, L. X. Zheng, L. P. Nie, T. Wu, and X. H. Chen, *Phys. Rev. Lett.* **125**, 097003 (2020).
- [11] B. D. Faeth, S.-L. Yang, J. K. Kawasaki, J. N. Nelson, P. Mishra, C. T. Parzyck, C. Li, D. G. Schlom, and K. M. Shen, *Phys. Rev. X* **11**, 021054 (2021).
- [12] S. Donovan, A. Schwartz, and G. Grüner, *Phys. Rev. Lett.* **79**, 1401 (1997).
- [13] B. B. Zhou, S. Misra, E. H. Da Silva Neto, P. Aynajian, R. E. Baumbach, J. D. Thompson, E. D. Bauer, and A. Yazdani, *Nature Physics* **9**, 474 (2013).
- [14] A. Gynis, B. E. Feldman, M. T. Randeria, G. A. Peterson, E. D. Bauer, P. Aynajian, and A. Yazdani, *Nat. Commun.* **9**, 549 (2018).
- [15] M. Oh, K. P. Nuckolls, D. Wong, R. L. Lee, X. Liu, K. Watanabe, T. Taniguchi, and A. Yazdani, *Nature* **600**, 240 (2021).
- [16] X. Li, S. Wang, X. Luo, Y.-Y. Zhou, K. Xie, H.-C. Shen, Y.-Z. Nie, Q. Chen, H. Hu, Y.-A. Chen, X.-C. Yao, and J.-W. Pan, *Nature* **626**, 288 (2024).
- [17] X.-C. Wang and Y. Qi, *Phys. Rev. B* **107**, 224502 (2023).
- [18] T. Yoshida, X. J. Zhou, T. Sasagawa, W. L. Yang, P. V. Bogdanov, A. Lanzara, Z. Hussain, T. Mizokawa, A. Fujimori, H. Eisaki, Z.-X. Shen, T. Kakeshita, and S. Uchida, *Phys. Rev. Lett.* **91**, 027001 (2003).
- [19] A. Kanigel, M. R. Norman, M. Randeria, U. Chatterjee, S. Souma, A. Kaminski, H. M. Fretwell, S. Rosenkranz, M. Shi, T. Sato, T. Takahashi, Z. Z. Li, H. Raffy, K. Kadowaki, D. Hinks, L. Ozyuzer, and J. C. Campuzano, *Nat. Phys.* **2**, 447 (2006).
- [20] A. Kanigel, U. Chatterjee, M. Randeria, M. R. Norman, S. Souma, M. Shi, Z. Z. Li, H. Raffy, and J. C. Campuzano, *Phys. Rev. Lett.* **99**, 157001 (2007).
- [21] T. Kondo, W. Malaeb, Y. Ishida, T. Sasagawa, H. Sakamoto, T. Takeuchi, T. Tohyama, and S. Shin, *Nat. Commun.* **6**, 7699 (2015).
- [22] J. M. Luttinger, *Phys. Rev.* **119**, 1153 (1960).
- [23] D. K. Singh, S. Kadge, Y. Bang, and P. Majumdar, *Phys. Rev. B* **105**, 054501 (2022).
- [24] H.-J. Kwon and A. T. Dorsey, *Phys. Rev. B* **59**, 6438 (1999).
- [25] M. Franz and A. J. Millis, *Phys. Rev. B* **58**, 14572 (1998).
- [26] S. Banerjee, T. V. Ramakrishnan, and C. Dasgupta, *Phys. Rev. B* **84**, 144525 (2011).

\* xiaoyanxu@sjtu.edu.cn

[27] B. Keimer, S. A. Kivelson, M. R. Norman, S. Uchida, and J. Zaanen, *Nature* **518**, 179 (2015).

[28] Y. J. Uemura, G. M. Luke, B. J. Sternlieb, J. H. Brewer, J. F. Carolan, W. N. Hardy, R. Kadono, J. R. Kempton, R. F. Kiefl, S. R. Kreitzman, P. Mulhern, T. M. Riseman, D. L. Williams, B. X. Yang, S. Uchida, H. Takagi, J. Gopalakrishnan, A. W. Sleight, M. A. Subramanian, C. L. Chien, M. Z. Cieplak, G. Xiao, V. Y. Lee, B. W. Statt, C. E. Stronach, W. J. Kossler, and X. H. Yu, *Phys. Rev. Lett.* **62**, 2317 (1989).

[29] V. J. Emery and S. A. Kivelson, *Nature* **374**, 434 (1995).

[30] J. M. Kosterlitz and D. J. Thouless, *Journal of Physics C: Solid State Physics* **6**, 1181 (1973).

[31] J. M. Kosterlitz, *Journal of Physics C: Solid State Physics* **7**, 1046 (1974).

[32] Refer to the Supplemental Material at [URL](#) for detailed technical information on the following topics: the evaluation of electronic self-energy, pseudogap in the single-particle spectrum of electron, the implementation of determinant Quantum Monte Carlo simulation, the absence of antiferromagnetic order, the determination of BKT transition point, and the stochastic analytic continuation calculation.

[33] V. Kozii and L. Fu, *Phys. Rev. B* **109**, 235139 (2024).

[34] Y. Nagai, Y. Qi, H. Isobe, V. Kozii, and L. Fu, *Phys. Rev. Lett.* **125**, 227204 (2020).

[35] H. Shen, B. Zhen, and L. Fu, *Phys. Rev. Lett.* **120**, 146402 (2018).

[36] T. Yoshida, R. Peters, and N. Kawakami, *Phys. Rev. B* **98**, 035141 (2018).

[37] Y. Michishita, T. Yoshida, and R. Peters, *Phys. Rev. B* **101**, 085122 (2020).

[38] J. F. Annett, *Superconductivity, Superfluids and Condensates*, 1st ed. (Oxford University, Oxford, 2003).

[39] X. Y. Xu and T. Grover, *Phys. Rev. Lett.* **126**, 217002 (2021).

[40] S. Sachdev, *Quantum Phase Transitions*, 2nd ed. (Cambridge University Press, 2011).

[41] C. Wu and S.-C. Zhang, *Phys. Rev. B* **71**, 155115 (2005).

[42] F. Assaad and H. Evertz, *Computational Many-Particle Physics*, edited by H. Fehske, R. Schneider, and A. Weiße, Lecture Notes in Physics, Vol. 739 (Springer, Berlin, Heidelberg, 2008) pp. 277–356.

[43] A. W. Sandvik, *Phys. Rev. B* **57**, 10287 (1998).

[44] H. Shao and A. W. Sandvik, *Phys. Rep.* **1003**, 1 (2023).

[45] G. D. Mahan, *Many-Particle Physics*, 3rd ed. (Springer, New York, 2000).

[46] M. R. Norman, M. Randeria, H. Ding, and J. C. Campuzano, *Phys. Rev. B* **57**, R11093 (1998).

[47] M. Shi, J. Chang, S. Pailhés, M. R. Norman, J. C. Campuzano, M. Måansson, T. Claesson, O. Tjernberg, A. Bendounan, L. Patthey, N. Momono, M. Oda, M. Ido, C. Mudry, and J. Mesot, *Phys. Rev. Lett.* **101**, 047002 (2008).

[48] M. V. Sadovskii, Sov. Phys. JETP **39**, 845 (1974).

[49] M. V. Sadovskii, Sov. Phys. JETP **50**, 989 (1979).

[50] R. H. McKenzie and D. Scarratt, *Phys. Rev. B* **54**, R12709 (1996).

[51] J. Schmalian, D. Pines, and B. Stojković, *Phys. Rev. Lett.* **80**, 3839 (1998).

[52] J. Schmalian, D. Pines, and B. Stojković, *Phys. Rev. B* **60**, 667 (1999).

[53] D. J. Scalapino, *Rev. Mod. Phys.* **84**, 1383 (2012).

[54] P. Dai, *Rev. Mod. Phys.* **87**, 855 (2015).

[55] F. F. Assaad, *Phys. Rev. B* **71**, 075103 (2005).

[56] W. Jiang, Y. Liu, A. Klein, Y. Wang, K. Sun, A. V. Chubukov, and Z. Y. Meng, *Nat. Commun.* **13**, 2655 (2022).

[57] U. Wolff, *Phys. Rev. Lett.* **62**, 361 (1989).

[58] W. Jiang, G. Pan, Y. Liu, and Z.-Y. Meng, *Chinese Physics B* **31**, 040504 (2022).

[59] M. S. S. Challa and D. P. Landau, *Phys. Rev. B* **33**, 437 (1986).

**Supplementary Material for “The interplay of phase fluctuations and nodal quasiparticles: ubiquitous Fermi arcs in two-dimensional *d*-wave superconductors”**

**CONTENTS**

I. Perturbative Evaluation of the Electronic Self-energy	1
II. Evolution of Electronic Single-particle Spectrum and the Pseudogap	2
III. Implementation of Determinant Quantum Monte Carlo Algorithm	4
A. Basic Formalism of Determinant Quantum Monte Carlo	4
B. Monte Carlo Updating Schemes	6
C. Measurements	7
IV. Absence of Antiferromagnetic Order	8
V. Determination of the BKT Transition Point	8
VI. Stochastic Analytic Continuation Calculation	9

**I. PERTURBATIVE EVALUATION OF THE ELECTRONIC SELF-ENERGY**

In this section, we derive the electronic self-energy of phase-disordered superconductor by combining perturbation theory and disorder-average technique [S45]. Due to the disorder-average condition  $\Delta(\mathbf{r}) = \Delta^*(\mathbf{r}) = 0$ , the first-order correction simply vanishes. Hence we concentrate on the second-order correction, which follows straightforwardly from the Feynman diagram in Fig. S1, and is written down as

$$\Sigma(\mathbf{k}, \mathbf{k}', \omega) = \frac{1}{V} \int \frac{d^2 \mathbf{p}}{(2\pi)^2} \frac{\Delta_{\mathbf{k}\mathbf{p}} \Delta_{\mathbf{p}\mathbf{k}'}^*}{\omega + \xi_p + i0^+}, \quad (\text{S1})$$

where the spin index has been omitted since the self-energy is trivial in the spin subspace.

The self-energy Eq. (S1) depends on both the incoming momentum  $\mathbf{k}$  and the outgoing one  $\mathbf{k}'$  because the translational invariance is explicitly broken for certain fixed pairing configurations  $\{\Delta(\mathbf{r}, \mathbf{s})\}$ . The Fourier-transformed pairing order parameter  $\Delta_{\mathbf{k}\mathbf{p}}$  is defined as

$$\begin{aligned} \Delta_{\mathbf{p}_1 \mathbf{p}_2} &= \int d^2 \mathbf{r} d^2 \mathbf{s} \Delta(\mathbf{r}, \mathbf{s}) e^{-i\mathbf{p}_1(\mathbf{r}+\mathbf{s}/2) - i\mathbf{p}_2(\mathbf{r}-\mathbf{s}/2)} \\ &= \int d^2 \mathbf{r} \Delta(\mathbf{r}) e^{-i(\mathbf{p}_1 + \mathbf{p}_2)\mathbf{r}} \varphi\left(\frac{\mathbf{p}_1 - \mathbf{p}_2}{2}\right), \end{aligned} \quad (\text{S2})$$

where in the second step we have applied the relation  $\int d^2 \mathbf{s} e^{-i\mathbf{p}\mathbf{s}} \Delta(\mathbf{r}, \mathbf{s}) = \Delta(\mathbf{r}) \varphi(\mathbf{p})$ . Hereafter, we will assume a *d*-wave form factor  $\varphi(\mathbf{p}) = (p_x^2 - p_y^2)/p^2$ , but note that a similar analysis can be conducted to deal with generic pairing symmetries. In addition, for the convenience of analytic calculation and without losing of generality, we adopt a Gaussian decay function  $g(|\mathbf{r} - \mathbf{r}'|/\xi) = e^{-|\mathbf{r} - \mathbf{r}'|^2/2\xi^2}$  for the disorder-averaged two-point pairing correlation in

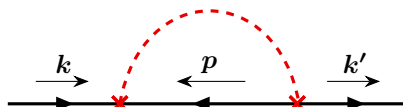


FIG. S1. Feynman diagram for the second-order self-energy correction. The arrowed solid lines denote the bare propagators of band electrons, while the dashed red line represents the disorder average over the fluctuating pairing correlations.

Eq. (2b), and express it in the momentum space as

$$\begin{aligned} \overline{\Delta_{\mathbf{p}_1 \mathbf{p}_2} \Delta_{\mathbf{p}_3 \mathbf{p}_4}^*} &= \int d^2 \mathbf{r}_1 d^2 \mathbf{r}_2 \overline{\Delta(\mathbf{r}_1) \Delta(\mathbf{r}_2)^*} e^{-i(\mathbf{p}_1 + \mathbf{p}_2) \cdot \mathbf{r}_1 + i(\mathbf{p}_3 + \mathbf{p}_4) \cdot \mathbf{r}_2} \varphi\left(\frac{\mathbf{p}_1 - \mathbf{p}_2}{2}\right) \varphi^*\left(\frac{\mathbf{p}_3 - \mathbf{p}_4}{2}\right) \\ &= 2\pi\xi^2 \Delta_0^2 V \delta^{(2)}(\mathbf{p}_1 + \mathbf{p}_2 - \mathbf{p}_3 - \mathbf{p}_4) e^{-(\mathbf{p}_1 + \mathbf{p}_2)^2 \xi^2/2} \varphi\left(\frac{\mathbf{p}_1 - \mathbf{p}_2}{2}\right) \varphi^*\left(\frac{\mathbf{p}_3 - \mathbf{p}_4}{2}\right). \end{aligned} \quad (\text{S3})$$

Substituting this result into Eq. (S1), we obtain the disorder-averaged self-energy  $\overline{\Sigma(\mathbf{k}, \mathbf{k}', \omega)} = \Sigma(\mathbf{k}, \omega) \delta^{(2)}(\mathbf{k} - \mathbf{k}')$  with

$$\Sigma(\mathbf{k}, \omega) = 2\pi\xi^2 \Delta_0^2 \int \frac{d^2 \mathbf{p}}{(2\pi)^2} \frac{e^{-(\mathbf{k} + \mathbf{p})^2 \xi^2/2}}{\omega + \xi_p + i0^+} \left| \varphi\left(\frac{\mathbf{k} - \mathbf{p}}{2}\right) \right|^2. \quad (\text{S4})$$

As expected, the translational invariance is recovered after averaging over the fluctuating pairing potential. From Eq. (S4), one can already realize that the self-energy acquires a finite imaginary component due to the scattering mediated by phase fluctuations, contributing to the finite life-time of Cooper pairs. This can be brought out explicitly by further considering the weakly fluctuating regime with  $k_F \xi \gg 1$ , or equivalently temperature range near  $T_c$  in the normal state, and examining the imaginary part of Eq. (S4),

$$\begin{aligned} \text{Im}\Sigma(\mathbf{k}, \omega) &\approx 2\pi\xi^2 |\Delta_{\mathbf{k}}|^2 \int \frac{d^2 \mathbf{p}}{(2\pi)^2} e^{-(\mathbf{k} + \mathbf{p})^2 \xi^2/2} [-\pi\delta(\omega + \xi_p)] \\ &= -\pi m \xi^2 |\Delta_{\mathbf{k}}|^2 e^{-\xi^2 k^2 + m \xi^2 (\omega + \xi_k)} I_0\left(\xi^2 k^2 \sqrt{1 - \frac{2m}{k^2}(\omega + \xi_k)}\right), \quad \text{with } \omega < \mu \\ &\approx -\pi |\Delta_{\mathbf{k}}|^2 \frac{m\xi}{(2\pi)^{1/2} k} e^{-\frac{m^2 \xi^2}{2k^2} (\omega + \xi_k)^2}. \end{aligned} \quad (\text{S5})$$

For finally arriving at Eq. (S5), we first observe that the integrand in Eq. (S4) takes significant value only for a small portion of momenta around  $\mathbf{p} = -\mathbf{k}$  with a soft cutoff  $\xi^{-1}$ . This allows us to substitute  $\varphi[(\mathbf{k} - \mathbf{p})/2]$  in Eq. (S4) with  $\varphi[\mathbf{k}]$ , and further absorb it into  $\Delta_{\mathbf{k}}$  in the first step of Eq. (S5). Also, we have used the identity  $\text{Im}[1/(\omega + \xi_p + i0^+)] = -\pi\delta(\omega + \xi_p)$ . In the second step, the integral over  $\mathbf{p}$  is solved exactly by assuming the dispersion  $\xi_k = k^2/2m - \mu$ , and  $I_0$  is the zero-order modified Bessel function of the first kind. The asymptotic form of  $I_0$  in the  $k_F \xi \gg 1$  limit is adopted in the last step, and it is finally found that the imaginary part of self-energy obeys a Gaussian distribution peaking at  $\omega = -\xi_k$  with the standard deviation  $\sigma = 2\gamma_{\mathbf{k}} \equiv k/m\xi$ .

Eq. (S5) then motivates us to intuitively rewrite the self-energy Eq. (S4) in the weakly fluctuating regime as

$$\Sigma(\mathbf{k}, \omega) = \frac{|\Delta_{\mathbf{k}}|^2}{\omega + \xi_k + 2i\gamma_{\mathbf{k}}}, \quad (\text{S6})$$

which is exactly what we have announced in the main text. The imaginary part of Eq. (S6) now obeys a Lorentz distribution as compared with the Gaussian one in Eq. (S5). For temperature  $T$  close to  $T_c$  in the normal state, it is plausible that Eq. (S4) and Eq. (S6) shall behave similarly. To see this, both the real and imaginary parts of Eq. (S4) and Eq. (S6) are benchmarked numerically in Fig. S2, where good agreements are achieved for  $k_F \xi \gg 1$ . We argue that for any specific form of two-point pairing correlation  $g(r/\xi)$ , the detailed high-energy information of the correlation decay can hardly be probed in the vicinity of  $T_c$ , and hence turns out to be irrelevant. Under this assumption, a similar analysis as we outline above can be applied for generic pairing correlations, and it is generally expected that the effects of weak phase fluctuations shall be well captured by the self-energy in Eq. (S6).

## II. EVOLUTION OF ELECTRONIC SINGLE-PARTICLE SPECTRUM AND THE PSEUDOGAP

Following directly from the self-energy in Eq. (S6), the retarded Green's function is written down as

$$G(\mathbf{k}, \omega) = \frac{\omega + \xi_k + 2i\gamma_{\mathbf{k}}}{\omega^2 - E_k^2 + 2i\gamma_{\mathbf{k}}(\omega - \xi_k)}, \quad (\text{S7})$$

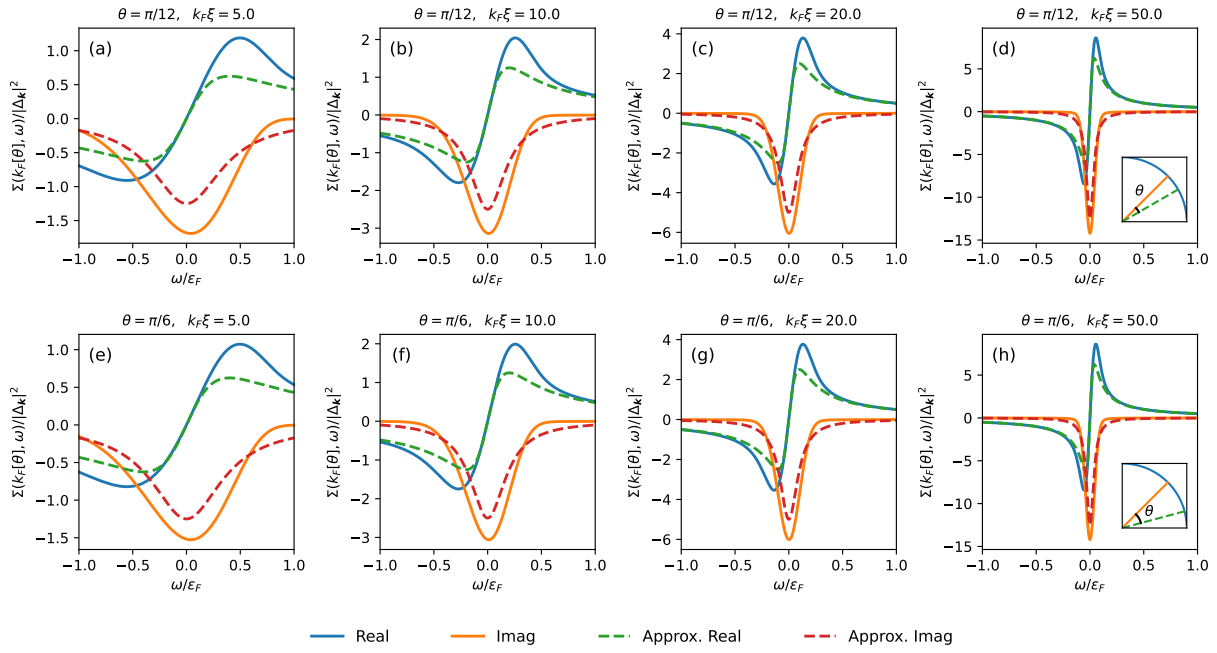


FIG. S2. Benchmark of self-energies in Eq. (S4) and Eq. (S6) by varying both the correlation length  $\xi$  and the Fermi momentum  $\mathbf{k}_F[\theta]$ .  $\theta$  denotes the angle to the  $d$ -wave node, as illustrated in the mini charts of the rightmost figures. The exact self-energies, Eq. (S4), are plotted in solid lines while the approximated ones, Eq. (S6), are in dashed lines. It is found that Eq. (S6) produces similar real and imaginary components as those of Eq. (S4), especially when  $k_F\xi$  grows up. We have also tested Eq. (S6) for momenta away from the Fermi surface, which only cause a frequency shift as compared to the results above, and hence we do not show them separately.

where we define the  $d$ -wave BCS dispersion  $E_k = \sqrt{\xi_k^2 + |\Delta_k|^2}$ . The quasiparticle dispersion, Eq. (4), in the presence of phase fluctuations is embedded in the complex poles of Green's function, which are readily read from Eq. (S7). The single-particle spectral function  $A(\mathbf{k}, \omega)$  is related to the imaginary component of  $G(\mathbf{k}, \omega)$  as

$$A(\mathbf{k}, \omega) = -2\text{Im}[G(\mathbf{k}, \omega)] = \frac{4|\Delta_k|^2 \gamma_{\mathbf{k}}}{(\omega^2 - E_k^2)^2 + 4\gamma_{\mathbf{k}}^2 (\omega - \xi_k)^2}, \quad (\text{S8})$$

and for Fermi momentum  $\mathbf{k}_F$  with  $\xi_{\mathbf{k}_F} = 0$ ,

$$A(\mathbf{k}_F, \omega) = \frac{4|\Delta_k|^2 \gamma}{\left(\omega^2 - |\Delta_k|^2\right)^2 + 4\gamma^2 \omega^2}, \quad (\text{S9})$$

where the pair-scattering rate  $\gamma = v_F/2\xi$ . By examining the denominator of Eq. (S9), it is easy to find that  $A(\mathbf{k}_F, \omega)$  reaches its maximum when

$$\omega = 0, \quad \gamma/|\Delta_k| \geq 1/\sqrt{2}; \quad (\text{S10a})$$

$$\omega = \pm \sqrt{|\Delta_k|^2 - 2\gamma^2}, \quad \gamma/|\Delta_k| < 1/\sqrt{2}. \quad (\text{S10b})$$

According to these observations, we define the energy scale of pseudogap  $\Delta_{\text{pg}}(\mathbf{k}) = \sqrt{|\Delta_k|^2 - 2\gamma^2}$ . It is then realized that above  $T_c$  in the normal state, the spectral gap remains open unless  $\gamma/|\Delta_k| \geq 1/\sqrt{2}$ . The smooth crossover from the BCS physics when  $T \gtrsim T_c$  to the high-temperature Fermi liquid when  $T \gg T_c$ , i.e. the evolution of pseudogap, is depicted in Fig. S3(a). In the weakly fluctuating regime with  $\gamma \ll |\Delta_k|$ , we infer from Eq. (S9) that  $A_{\pm}(\mathbf{k}_F, \omega) \approx \gamma / \left[ (\omega \pm |\Delta_k|)^2 + \gamma^2 \right]$ , where the half-width broadening of BCS quasiparticle weights  $A(|\omega| \sim |\Delta_k|)$  are simply characterized by  $\gamma$ , as shown in Fig. S3(b).

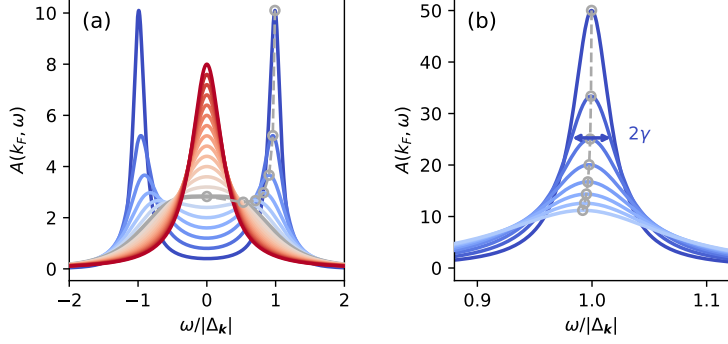


FIG. S3. Single-particle spectral function  $A(\mathbf{k}_F, \omega)$  at the Fermi momentum for varying  $\gamma/|\Delta_{\mathbf{k}}|$ . We outline the spectral peaks at  $\omega = \Delta_{\text{pg}} = \sqrt{|\Delta_{\mathbf{k}}|^2 - 2\gamma^2}$  using the dashed line with circles. (a) The crossover from the BCS physics ( $\gamma \lesssim |\Delta_{\mathbf{k}}|$ ) to the Fermi liquid ( $\gamma \gtrsim |\Delta_{\mathbf{k}}|$ ) with  $\gamma/|\Delta_{\mathbf{k}}|$  ranging from  $10^{-1}$  to 2. The pseudogap develops in the intermediate regime of this crossover, and the energy gap is fully closed when  $\gamma/|\Delta_{\mathbf{k}}| = 1/\sqrt{2}$ , noted as the grey solid curve. (b) Broadening of the BCS quasiparticle peak, e.g.  $A(\omega \approx |\Delta_{\mathbf{k}}|)$ , in the weakly fluctuating regime for  $\gamma/|\Delta_{\mathbf{k}}|$  ranging from  $2 \times 10^{-2}$  to  $10^{-1}$ . The two-sided arrow implies that the spectral peak acquires a half-width proportional to  $\gamma$ .

### III. IMPLEMENTATION OF DETERMINANT QUANTUM MONTE CARLO ALGORITHM

#### A. Basic Formalism of Determinant Quantum Monte Carlo

We transcribe the Hubbard-like model  $H = H_t + H_U + H_V + H_{XY}$  in the main text as follows

$$H_t = -t \sum_{\langle ij \rangle, \sigma} (c_{i\sigma}^\dagger c_{j\sigma} + \text{h.c.}), \quad (\text{S11a})$$

$$H_U = \frac{U}{2} \sum_i (\rho_{i\uparrow} + \rho_{i\downarrow} - 1)^2, \quad (\text{S11b})$$

$$H_V = V \sum_{\langle ij \rangle} \left[ \tau_{ij} e^{i\theta_{ij}} (c_{i\uparrow}^\dagger c_{j\downarrow}^\dagger - c_{i\downarrow}^\dagger c_{j\uparrow}^\dagger) + \text{h.c.} \right], \quad (\text{S11c})$$

$$H_{XY} = K \sum_{\langle ij \rangle} \hat{L}_{ij}^2 - J \sum_{\langle ijk \rangle} \cos(\theta_{ij} - \theta_{jk}). \quad (\text{S11d})$$

In order to investigate the thermodynamic properties of this model, we perform determinant Quantum Monte Carlo (DQMC) simulation at finite temperatures. It is insightful to first switch to the particle-hole channel, and reformulate the model Hamiltonian on the square lattice with a basis transformation  $(\tilde{c}_{i\uparrow}^\dagger, \tilde{c}_{i\downarrow}^\dagger) \equiv (c_{i\uparrow}^\dagger, (-)^i c_{i\downarrow}^\dagger)$ . This gives rise to

$$H_t = -t \sum_{\langle ij \rangle, \sigma} (\tilde{c}_{i\sigma}^\dagger \tilde{c}_{j\sigma} + \text{h.c.}), \quad (\text{S12a})$$

$$H_U = -\frac{U}{2} \sum_i (\tilde{\rho}_{i\uparrow} + \tilde{\rho}_{i\downarrow} - 1)^2, \quad (\text{S12b})$$

$$H_V = -V \sum_{\langle ij \rangle} \left[ \tau_{ij} e^{i\theta_{ij}} (-)^i (\tilde{c}_{i\uparrow}^\dagger \tilde{c}_{j\downarrow} - \tilde{c}_{j\uparrow}^\dagger \tilde{c}_{i\downarrow}) + \text{h.c.} \right], \quad (\text{S12c})$$

$$H_{XY} = K \sum_{\langle ij \rangle} \hat{L}_{ij}^2 - J \sum_{\langle ijk \rangle} \cos(\theta_{ij} - \theta_{jk}), \quad (\text{S12d})$$

where  $\tilde{\rho}_{i\sigma} = \tilde{c}_{i\sigma}^\dagger \tilde{c}_{i\sigma}$  denotes the density operator in the particle-hole basis. Within the framework of DQMC and given the partition function  $\mathcal{Z} = \text{Tr}(e^{-\beta H})$ , one first divides the imaginary-time evolution  $\beta$  into  $N_\tau$  slices with imaginary-time spacing  $\Delta\tau = \beta/N_\tau$ . To further isolate the quartic interaction terms from the quadratic ones, we

decompose the exponent of  $H$  at certain time slice  $\tau$  into more components, where different components basically do not commute. This is fulfilled by applying Trotter decomposition at the cost of an accompanying systematic error of order  $O[(\Delta\tau)^2]$ , as in Eq. (S13),

$$\mathcal{Z} = \text{Tr} \left[ \left( e^{-\Delta\tau H} \right)^{N_\tau} \right] \approx \text{Tr} \left[ \left( e^{-\Delta\tau H_{XY}} e^{-\Delta\tau H_U} e^{-\Delta\tau H_V} e^{-\Delta\tau H_t} \right)^{N_\tau} \right]. \quad (\text{S13})$$

To analytically integrate out the fermionic degrees of freedom, one needs to transform the two-body interaction term  $H_U$  into fermion bilinears under the Hubbard-Stratonovich (HS) transformation. The resulting fermion bilinears are coupled to certain auxiliary bosonic fields  $\{s_{i,\tau}\}$ , which take values in  $\{\pm 1, \pm 2\}$  [S55],

$$e^{-\Delta\tau H_U(\tau)} = \prod_i e^{\Delta\tau \frac{U}{2} [\tilde{\rho}_{i\uparrow}(\tau) + \tilde{\rho}_{i\downarrow}(\tau) - 1]^2} \approx \frac{1}{4^N} \prod_i \sum_{s_{i,\tau}} \gamma(s_{i,\tau}) e^{\alpha\eta(s_{i,\tau}) [\tilde{\rho}_{i\uparrow}(\tau) + \tilde{\rho}_{i\downarrow}(\tau) - 1]}, \quad (\text{S14})$$

where  $N = L \times L$  counts the total number of lattice sites,  $\alpha = \sqrt{\Delta\tau \frac{U}{2}}$ ,  $\gamma(\pm 1) = 1 + \sqrt{6}/3$ ,  $\gamma(\pm 2) = 1 - \sqrt{6}/3$ ,  $\eta(\pm 1) = \pm\sqrt{6 - 2\sqrt{6}}$ , and  $\eta(\pm 2) = \pm\sqrt{6 + 2\sqrt{6}}$ . This particular scheme of HS transformation preserves the spin  $\mathbb{SU}(2)$  symmetry and introduces a systematic error of order  $O[(\Delta\tau)^3]$  when physical observables are measured, which is however neglectable compared with the Trotter error.

To deal with the bosonic rotor fields  $\hat{\theta}_{ij}$  present in  $H_{XY}$  in the path integral formalism, it is convenient to adopt the bosonic coherent state representation  $\{|\theta\rangle\}$  satisfying  $\hat{\theta}_{ij}|\theta\rangle = \theta_{ij}|\theta\rangle$  for all bonds  $\langle ij \rangle$ . Then our remaining task is to estimate the matrix elements  $\langle \theta' | e^{-\Delta\tau K} \sum_{\langle ij \rangle} \hat{L}_{ij}^2 | \theta \rangle$ . This can be achieved by inserting the completeness relation of angular momentum eigenstates  $\{|L\rangle\}$  and applying the Poisson summation formula [S56]. As a result, under the Villain approximation, we will arrive at

$$\langle \theta' | e^{-\Delta\tau K} \sum_{\langle ij \rangle} \hat{L}_{ij}^2 | \theta \rangle \sim e^{\frac{1}{2\Delta\tau K} \sum_{\langle ij \rangle} \cos(\theta_{ij} - \theta'_{ij})}. \quad (\text{S15})$$

After all these preparations, we are now ready to evaluate the partition function in Eq. (S13). First of all, we trace out the bosonic fields using Eq. (S15) and the properties of coherent states,

$$\begin{aligned} \mathcal{Z} &= \text{Tr}_F \sum_{\{\theta_{ij,\tau}\}} \langle \theta_{\tau=1} | e^{-\Delta\tau H} | \theta_{\tau=N_\tau} \rangle \langle \theta_{\tau=N_\tau} | e^{-\Delta\tau H} | \theta_{\tau=N_\tau-1} \rangle \cdots \langle \theta_{\tau=2} | e^{-\Delta\tau H} | \theta_{\tau=1} \rangle \\ &= \sum_{\{\theta_{ij,\tau}\}} e^{\frac{1}{2\Delta\tau K} \sum_{\langle ij \rangle, \tau} \cos(\theta_{ij,\tau+1} - \theta_{ij,\tau}) + \Delta\tau J \sum_{\langle ijk \rangle, \tau} \cos(\theta_{ij,\tau} - \theta_{jk,\tau})} \text{Tr}_F \left[ \prod_\tau \left( e^{-\Delta\tau H_U} e^{-\Delta\tau H_V} e^{-\Delta\tau H_t} \right) \right], \end{aligned} \quad (\text{S16})$$

where we have mapped the quantum rotor term  $H_{XY}$  into a (2+1)D anisotropic XY model at the path integral level. Furthermore, we trace out the fermion bilinears using Eq. (S14),

$$\begin{aligned} \text{Tr}_F \left[ \prod_\tau \left( e^{-\Delta\tau H_U} e^{-\Delta\tau H_V} e^{-\Delta\tau H_t} \right) \right] &= \sum_{\{s_{i,\tau}\}} \left( \prod_{i,\tau} \gamma(s_{i,\tau}) e^{-\alpha\eta(s_{i,\tau})} \right) \text{Tr}_F \left[ \prod_\tau \left( e^{\tilde{\mathbf{c}}^\dagger \mathbf{K}_U \tilde{\mathbf{c}}} e^{\tilde{\mathbf{c}}^\dagger \mathbf{K}_V \tilde{\mathbf{c}}} e^{\tilde{\mathbf{c}}^\dagger \mathbf{K}_t \tilde{\mathbf{c}}} \right) \right] \\ &= \sum_{\{s_{i,\tau}\}} \left( \prod_{i,\tau} \gamma(s_{i,\tau}) e^{-\alpha\eta(s_{i,\tau})} \right) \det \left( \mathbf{1} + \prod_\tau \mathbf{B}_\tau \right), \end{aligned} \quad (\text{S17})$$

with the constant prefactor omitted. In Eq. (S17),  $\tilde{\mathbf{c}} = (\tilde{c}_{1,\uparrow}, \dots, \tilde{c}_{N,\uparrow}, \tilde{c}_{1,\downarrow}, \dots, \tilde{c}_{N,\downarrow})^T$  denotes our fermionic basis, and the three matrices  $\mathbf{K}_t$ ,  $\mathbf{K}_V$ ,  $\mathbf{K}_U$  satisfy that  $\tilde{\mathbf{c}}^\dagger \mathbf{K}_t \tilde{\mathbf{c}} = -\Delta\tau H_t$ ,  $\tilde{\mathbf{c}}^\dagger \mathbf{K}_V \tilde{\mathbf{c}} = -\Delta\tau H_V$ , and  $\tilde{\mathbf{c}}^\dagger \mathbf{K}_U \tilde{\mathbf{c}} = \sum_i \alpha\eta(s_{i,\tau}) [\tilde{\rho}_{i\uparrow}(\tau) + \tilde{\rho}_{i\downarrow}(\tau)]$ .  $\mathbf{B}_\tau$  matrix is defined as  $\mathbf{B}_\tau = e^{\mathbf{K}_U} e^{\mathbf{K}_V} e^{\mathbf{K}_t}$ . To obtain Eq. (S17), one has to notice that for fermion bilinears, the identity  $\text{Tr} [e^{\mathbf{c}^\dagger \mathbf{K}_1 \mathbf{c}} e^{\mathbf{c}^\dagger \mathbf{K}_2 \mathbf{c}} \cdots e^{\mathbf{c}^\dagger \mathbf{K}_n \mathbf{c}}] = \det (\mathbf{1} + e^{\mathbf{K}_1} e^{\mathbf{K}_2} \cdots e^{\mathbf{K}_n})$  holds.

To summarize the result, we identify the field configurations  $\{\theta, s\}$  as  $\mathcal{C}$ , and the partition function can finally be expressed as  $\mathcal{Z} = \sum_{\mathcal{C}} \omega_{\mathcal{C}}^I \omega_{\mathcal{C}}^{II}$  with

$$\omega_{\mathcal{C}}^I = e^{\frac{1}{2\Delta\tau K} \sum_{\langle ij \rangle, \tau} \cos(\theta_{ij,\tau+1} - \theta_{ij,\tau}) + \Delta\tau J \sum_{\langle ijk \rangle, \tau} \cos(\theta_{ij,\tau} - \theta_{jk,\tau})} \left( \prod_{i,\tau} \gamma(s_{i,\tau}) e^{-\alpha\eta(s_{i,\tau})} \right), \quad (\text{S18a})$$

$$\omega_{\mathcal{C}}^{II} = \det \left( \mathbf{1} + \prod_\tau \mathbf{B}_\tau \right). \quad (\text{S18b})$$

It is important to realize that  $\tilde{\mathbf{c}}^\dagger \mathbf{K}_t \tilde{\mathbf{c}}$ ,  $\tilde{\mathbf{c}}^\dagger \mathbf{K}_V \tilde{\mathbf{c}}$ ,  $\tilde{\mathbf{c}}^\dagger \mathbf{K}_U \tilde{\mathbf{c}}$  stay invariant under the anti-unitary transformation  $\mathcal{U}$ :  $c_{i,\sigma} \rightarrow \sigma(-)^i c_{i,-\sigma}^\dagger$ ,  $\sqrt{-1} \rightarrow -\sqrt{-1}$ , as mentioned in the main text. This anti-unitary symmetry guarantees that the determinant in Eq. (S18b) is positive for any configuration  $\mathcal{C}$ , and the sign problem does not appear [S41].

## B. Monte Carlo Updating Schemes

We adopt the local updating scheme to update the auxiliary field configuration  $\mathcal{C}$ . The accepting ratio  $R$  of the new configuration  $\mathcal{C}'$  from  $\mathcal{C}$  is given by the detailed balance principle as

$$R = \min \left\{ 1, \omega_{\mathcal{C}'}^I \omega_{\mathcal{C}'}^{II} / \omega_{\mathcal{C}}^I \omega_{\mathcal{C}}^{II} \right\}, \quad (\text{S19})$$

where the ratio  $\omega_{\mathcal{C}'}^I / \omega_{\mathcal{C}}^I$  can be calculated trivially. To evaluate  $\omega_{\mathcal{C}'}^{II} / \omega_{\mathcal{C}}^{II}$ , a nice result holds

$$\frac{\omega_{\mathcal{C}'}^{II}}{\omega_{\mathcal{C}}^{II}} = \det \left[ \mathbf{1} + \Delta (\mathbf{1} - \mathbf{G}(\tau, \tau)) \right], \quad (\text{S20})$$

where we define  $\Delta = \mathbf{B}'_\tau \mathbf{B}_\tau^{-1} - \mathbf{1}$ , and the equal-time Green's function  $\mathbf{G}(\tau, \tau) = (\mathbf{1} + \mathbf{B}(\tau, 0) \mathbf{B}(\beta, \tau))^{-1}$  with  $\mathbf{B}(\tau_2, \tau_1) = \prod_{\tau=\tau_1+1}^{\tau_2} \mathbf{B}_\tau$ . We emphasise that the Green's functions are crucial to both the Monte Carlo updates and the measurements of physical observables, hence we shall carry them around throughout the entire simulation. Once the new configuration  $\mathcal{C}'$  is accepted, the Green's function is updated accordingly as

$$\mathbf{G}'(\tau, \tau) = \mathbf{G}(\tau, \tau) \left[ \mathbf{1} + \Delta (\mathbf{1} - \mathbf{G}(\tau, \tau)) \right]. \quad (\text{S21})$$

For local updates,  $\Delta$  possesses a quite sparse structure: e.g. for local update  $s_{i,\tau} \rightarrow s'_{i,\tau}$ , it has only two non-zero diagonal elements; and for the update of rotor  $\theta_{ij,\tau} \rightarrow \theta'_{ij,\tau}$ ,  $\Delta$  also involves a limited number of elements, which does not scale with the system size  $N$  so long as checkerboard breakups are applied when  $e^{\mathbf{K}_V}$  is multiplied. Due to the sparseness of  $\Delta$ , the locally updated Green's function can be evaluated efficiently according to Eq. (S21) with the Sherman-Morrison-Woodbury formula [S42].

Apart from the local updates, we also develop a global updating scheme to update the rotors by cluster. Because the rotor fields serve as the order parameter concerned with the  $\mathbb{U}(1)$  symmetry breaking of superconductivity, the simulation under the local updating scheme suffers the critical slowing down, especially in the dSC phase at low temperatures with a relatively small  $\Delta\tau$ . To overcome this problem, we embed the Wolff algorithm [S57, S58] into the general framework of DQMC. The steps for the global updating scheme are sketched as follows:

- Randomly select certain rotor field  $\theta_{ij,\tau}$  as the starting point for growing the cluster.
- Construct the rotor cluster in both the spatial and temporal directions according to the rotor-relevant weight in  $\omega_{\mathcal{C}}^I$ , using the standard Wolff algorithm [S57].
- To fulfill the detailed balance, the trial cluster update is accepted based on a probability given by

$$\mathcal{A}_f(\mathcal{C} \rightarrow \mathcal{C}') = \min \left\{ 1, \omega_{\mathcal{C}'}^{II} / \omega_{\mathcal{C}}^{II} \right\}, \quad (\text{S22})$$

where  $\mathcal{C}'$  denotes the new configuration after the cluster update. Once the trial configuration is accepted, we update all the rotors in the cluster simultaneously, and this completes a Wolff cluster update.

Note that after each global update, we need to compute the updated Green's function from scratch, which is numerically expensive. In practice, we always combine the global updates with the local ones, e.g. performing a batch of global updates after several local Monte Carlo sweeps over the complete space-time lattice. It is found that in the *d*-wave superconducting (dSC) phase, the combined updating scheme with both local and Wolff cluster (WC) updates tremendously reduces the Markov time for the auxiliary fields reaching thermal equilibrium, and in addition exhibits a much shorter autocorrelation time for various observables as compared with the pure local updating scheme. In Fig. S4 we show the autocorrelation functions measured for representative observables with these two updating schemes.

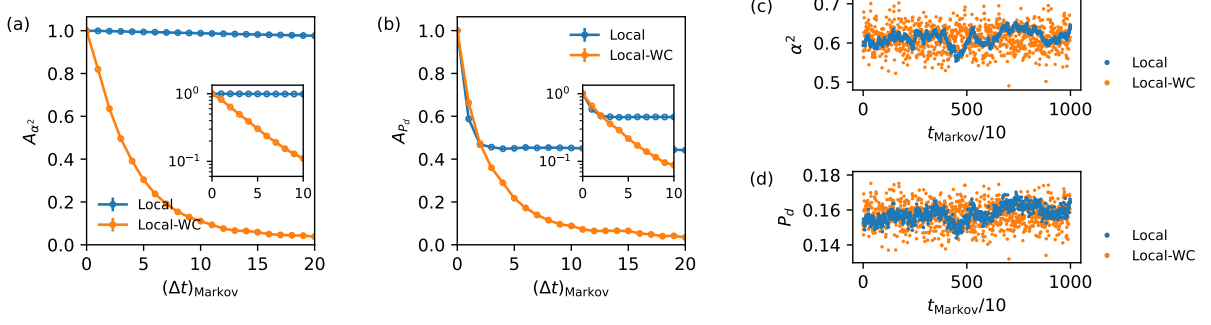


FIG. S4. Autocorrelation functions for the local updating scheme and the combined local-WC updating scheme. The autocorrelation function for certain observable  $O$  is defined as  $A_O(\Delta t) = [\langle O(t)O(t + \Delta t) \rangle - \langle O \rangle^2]/[\langle O^2 \rangle - \langle O \rangle^2]$ .  $\Delta t$  denotes the time difference on the Markov chain, and the Markov time  $t$  is measured in the unit of one single Monte Carlo sweep, where we scan over the complete space-time lattice for one time. In the local-WC scheme, one Wolff cluster move is followed after a local Monte Carlo sweep. Measurements are performed in the dSC phase with parameters  $L = 8$ ,  $\beta t = 2$ ,  $\Delta\tau t = 0.05$ ,  $t = 1$ ,  $U/t = 4$ ,  $V/t = 1$ , and  $K/t = J/t = 1/2$ . Under this setup, the local scheme typically suffers the critical slowing down. (a)(b) Autocorrelation function for (a) the bosonic pairing correlation  $\alpha^2$ , and (b) the fermionic pairing correlation  $P_d$ . The insets show the semi-log plots of the same data highlighting the exponentially decaying part of the autocorrelation. (c)(d) Typical sequences of  $\alpha^2$  and  $P_d$  as function of  $t_{\text{Markov}}$  in the equilibrium. Ten adjacent samples are regrouped for better visualization. The local-WC scheme generates nearly ‘randomly’ distributed sequences, justifying the statistical independence between samples. In contrast, the sequences generated by the local scheme show persistent correlations extending over thousands of Monte Carlo sweeps for both  $\alpha^2$  and  $P_d$ .

### C. Measurements

Both static and dynamic fermionic observables can be measured in DQMC by decomposing them into equal-time or time-displaced Green’s functions according to the Wick’s theorem. A standard Monte Carlo sampling procedure then follows to estimate the expectation values of these observables. For our purpose of detecting the  $d$ -wave superconductivity, we define the  $d$ -wave pairing order parameter  $\Delta_d = \frac{1}{2N} \sum_{\langle ij \rangle} \tau_{ij} (c_{j\downarrow} c_{i\uparrow} - c_{j\uparrow} c_{i\downarrow})$ , and measure the static  $d$ -wave pairing correlation function  $P_d$ ,

$$P_d \equiv \Delta_d \Delta_d^\dagger + \Delta_d^\dagger \Delta_d = \frac{1}{(2N)^2} \sum_{\langle ij \rangle, \langle kl \rangle} \tau_{ij} \tau_{kl} (-)^j (-)^l \left[ \left( \tilde{c}_{j\downarrow}^\dagger \tilde{c}_{i\uparrow} + \tilde{c}_{j\uparrow} \tilde{c}_{i\downarrow}^\dagger \right) \left( \tilde{c}_{k\uparrow}^\dagger \tilde{c}_{l\downarrow} + \tilde{c}_{k\downarrow} \tilde{c}_{l\uparrow}^\dagger \right) + \left( \tilde{c}_{k\uparrow}^\dagger \tilde{c}_{l\downarrow} + \tilde{c}_{k\downarrow} \tilde{c}_{l\uparrow}^\dagger \right) \left( \tilde{c}_{j\downarrow}^\dagger \tilde{c}_{i\uparrow} + \tilde{c}_{j\uparrow} \tilde{c}_{i\downarrow}^\dagger \right) \right], \quad (\text{S23})$$

where we have expressed the formula in the particle-hole channel, and identified the equal-time Green’s function in this basis as  $\mathbf{G}_{i\sigma, j\sigma'}(\tau, \tau) \equiv \langle \tilde{c}_{i\sigma}(\tau) \tilde{c}_{j\sigma'}^\dagger(\tau) \rangle$ . One then breaks up the quartic terms in Eq. (S23) into products of Green’s function using the Wick’s theorem.

Another important observable we desire to evaluate is the single-particle spectral function  $A_\sigma(\mathbf{k}, \omega)$ , through the measurement of which the formation of pseudogap and Fermi arcs are directly observed. Consider the time-displaced Green’s function in the momentum space,

$$G_\sigma(\mathbf{k}, \tau) \equiv \frac{1}{N} \sum_{ij} e^{-i\mathbf{k}(\mathbf{r}_i - \mathbf{r}_j)} \langle c_{i\sigma}(\tau) c_{j\sigma}^\dagger(0) \rangle = \begin{cases} \frac{1}{N} \sum_{ij} e^{-i\mathbf{k}(\mathbf{r}_i - \mathbf{r}_j)} \mathbf{G}_{i\sigma, j\sigma}(\tau, 0), & \sigma = \uparrow \\ -\frac{1}{N} \sum_{ij} e^{-i\mathbf{k}(\mathbf{r}_i - \mathbf{r}_j)} (-)^i (-)^j \mathbf{G}_{j\sigma, i\sigma}(0, \tau), & \sigma = \downarrow \end{cases} \quad (\text{S24})$$

where  $\mathbf{G}_{i\sigma, j\sigma'}(\tau, 0) \equiv \langle \tilde{c}_{i\sigma}(\tau) \tilde{c}_{j\sigma'}^\dagger(0) \rangle$  and  $\mathbf{G}_{i\sigma, j\sigma'}(0, \tau) \equiv \langle \tilde{c}_{i\sigma}(0) \tilde{c}_{j\sigma'}^\dagger(\tau) \rangle = -\langle \tilde{c}_{j\sigma'}^\dagger(\tau) \tilde{c}_{i\sigma}(0) \rangle$ . The imaginary-time Green’s function  $G_\sigma(\mathbf{k}, \tau)$  is directly measurable in DQMC, while  $A_\sigma(\mathbf{k}, \omega)$  is not. In fact, the single-particle spectrum  $A_\sigma(\mathbf{k}, \omega)$  is related to  $G_\sigma(\mathbf{k}, \tau)$  through an integral transform, for obtaining which we perform the stochastic analytic continuation calculations, as we will introduce below in Sec. VI.

#### IV. ABSENCE OF ANTIFERROMAGNETIC ORDER

It is shown in this section that in our explored parameter region of the Hubbard-like model, there is vanishing antiferromagnetic order (AFM) at finite temperatures although strong on-site electron repulsion is present. The AFM order parameter is defined as  $\vec{m} = \frac{1}{N} \sum_i (-)^i \vec{S}_i$ , with the static correlation

$$m^2 = \frac{1}{N^2} \sum_{ij} (-)^i (-)^j \langle \vec{S}_i \cdot \vec{S}_j \rangle. \quad (\text{S25})$$

$\vec{S}_i = \frac{1}{2} \sum_{\alpha\beta} \vec{\sigma}_{\alpha\beta} c_{i\alpha}^\dagger c_{i\beta}$  denotes the electron spin at site  $i$ , and  $\sigma^a$  are three Pauli matrices for  $a = x, y, z$ . The spin correlation is then expressed in terms of fermion operators,

$$\begin{aligned} \vec{S}_i \cdot \vec{S}_j &= \frac{1}{4} (\rho_{i\uparrow} - \rho_{i\downarrow})(\rho_{j\uparrow} - \rho_{j\downarrow}) + \frac{1}{2} \sum_{\alpha} c_{i\alpha}^\dagger c_{i\alpha} c_{j\bar{\alpha}}^\dagger c_{j\bar{\alpha}} \\ &= \frac{1}{4} (\tilde{\rho}_{i\uparrow} + \tilde{\rho}_{i\downarrow} - 1)(\tilde{\rho}_{j\uparrow} + \tilde{\rho}_{j\downarrow} - 1) + \frac{1}{2} (-)^i (-)^j \left( \tilde{c}_{i\uparrow}^\dagger \tilde{c}_{i\downarrow}^\dagger \tilde{c}_{j\downarrow} \tilde{c}_{j\uparrow} + \tilde{c}_{i\downarrow} \tilde{c}_{i\uparrow} \tilde{c}_{j\uparrow}^\dagger \tilde{c}_{j\downarrow}^\dagger \right), \end{aligned} \quad (\text{S26})$$

where the two-body correlations involved are now ready to be broken down into products of one-body Green's functions in the particle-hole basis. In Fig. S5, we measure the static AFM correlation  $m^2$  as a function of  $\beta$  and  $L$ . As adopted in the main text, we have set  $t = 1$ ,  $U/t = 4$ ,  $V/t = 1$ ,  $K/t = J/t = 1/2$ , and  $\Delta\tau = 0.025/t$ . The examined temperature range covers both dSC phase and the normal state that we explored. In Fig. S5(b), the value of  $m^2$  in the thermodynamic limit is estimated by extrapolating  $m^2(L)$  to  $1/L \rightarrow 0$ , which proves the absence of AFM order.

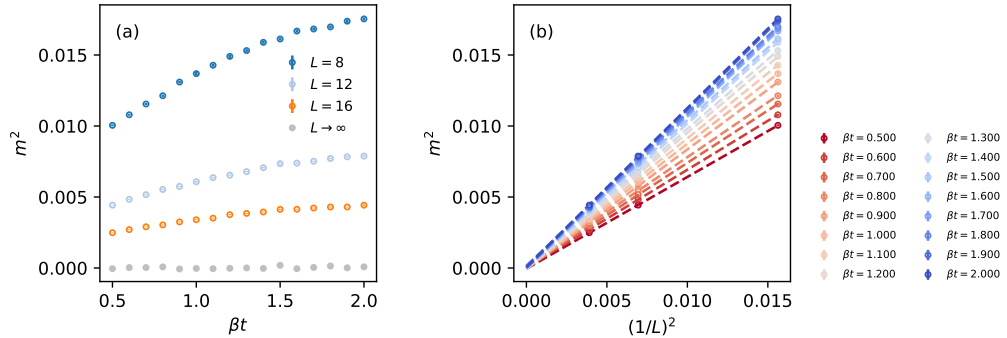


FIG. S5. Suppression of static AFM correlation  $m^2$ .

#### V. DETERMINATION OF THE BKT TRANSITION POINT

The precise determination of BKT transition point requires careful finite-size scaling analysis. According to the finite-size-scaling theory [S59], the scaling of the  $d$ -wave pairing correlation  $P_d$  follows a BKT form

$$P_d L^{\eta(T_c)} = f \left[ \exp(bt_r^{-1/2})/L \right], \quad \xi \sim \exp \left( bt_r^{-1/2} \right). \quad (\text{S27})$$

$t_r = T/T_c - 1$  denotes the reduced temperature, and  $f$  is a universal scaling function. The critical exponent is  $\eta(T_c) = 1/4$  for the BKT transition. For the bosonic correlation  $\alpha^2$ , an identical relation as in Eq. (S27) applies. At  $T = T_c$  where the correlation length  $\xi$  diverges, it is inferred from Eq. (S27) that  $P_d L^{\eta(T_c)}$  for varying  $L$  shall coincide at  $T_c$ . In DQMC simulations, the  $d$ -wave pairing correlation  $P_d(L, \beta)$  is measured for varying temperatures and system sizes. It is thus expected that  $P_d(L, \beta) L^{\eta(T_c)}$  converge at  $\beta_c$  for all  $L$ , which allows us to precisely locate the transition temperature  $\beta_c$ , as what we have done in Fig. 3 of the main text. Given the  $\beta_c$  obtained above, one then tunes the non-universal factor  $b$  to let the  $P_d(L, \beta)$  data for all  $\beta$  and  $L$  collapse into a universal function according to Eq. (S27). Once the value of  $b$  is determined, the correlation length  $\xi$  follows as  $\xi \sim \exp(bt_r^{-1/2})$ .

## VI. STOCHASTIC ANALYTIC CONTINUATION CALCULATION

As mentioned in Sec. III C, it is a technically challenging task to evaluate the single-particle spectrum  $A(\omega)$  from the imaginary-time Green's function  $G(\tau)$ , which is defined on a set of discrete imaginary-time points  $\{\tau\}$ . By definition,  $G(\tau)$  is related to  $A(\omega)$  through the following integral transform

$$G(\tau) = \int d\omega A(\omega) K(\tau, \omega), \quad (\text{S28})$$

where  $K(\tau, \omega)$  denotes the integral kernel. For fermionic Green's function,  $K(\tau, \omega) = e^{-\tau\omega} / (1 + e^{-\beta\omega})$ . It has long been realized that solving the inverse integral transform, i.e. obtaining  $A(\omega)$  from  $G(\tau)$ , appears to be an ill-posed problem. Practically,  $G(\tau)$ 's are always estimated from the QMC simulations with certain statistical errors, which makes the analytic continuation procedure numerically unstable.

To overcome this challenge, we apply the stochastic analytic continuation (SAC) [S43] algorithm to obtain all the single-particle spectra presented in this work. The combination of QMC and SAC has been proved reliable in recovering the real-frequency spectral functions among a wide class of spin and fermionic models. For interested readers, we refer to a recent review [S44], which provides a comprehensive introduction to SAC. The key spirit of SAC is to perform a Monte Carlo sampling procedure over the parametric space of  $A(\omega)$ . The statistical weight of certain parametric configuration  $\mathcal{C}_A$  is assumed to obey a Boltzmann distribution,

$$W_{\mathcal{C}_A} \sim \exp\left(-\frac{\chi^2}{2\Theta}\right), \quad (\text{S29})$$

where  $\chi^2$  quantifies the goodness of fitting between the QMC-measured Green's functions and the ones computed from the parameterized spectrum.  $\Theta$  represents the fictitious temperature that serves to balance the minimization of  $\chi^2$  and the 'thermal' fluctuations, which help to smooth the spectrum. In practice, one performs a simulated annealing procedure to lower  $\Theta$  adiabatically from a sufficiently high value. Once the optimal  $\Theta$  is found according to certain criteria, all statistically equivalent spectral configurations are sampled to produce the final real-frequency spectrum.